




Article

The Role of Oxygenated Functional Groups on Cadmium Removal using Pyrochar and Hydrochar Derived from *Guadua angustifolia* Residues

Carlos Navas-Cárdenas ^{1,2,*}, Manuel Caetano ¹, Diana Endara ³, Rocío Jiménez ², Ana B. Lozada ³, Lucía E. Manangón ³, Angélica Navarrete ², Carlos Reinoso ⁴, Alicia E. Sommer-Márquez ¹ and Yanet Villasana ²

¹ School of Chemical Sciences & Engineering, Yachay Tech University, Urcuquí 100119, Ecuador

² Biomass Laboratory, Biomass to Resources Group, Universidad Regional Amazónica Ikiam, Tena 096975, Ecuador

³ Department of Extractive Metallurgy, Escuela Politécnica Nacional, Quito 170517, Ecuador

⁴ School of Physical Sciences & Nanotechnology, Yachay Tech University, Urcuquí 100119, Ecuador

* Correspondence: cnavas@yachaytech.edu.ec

Abstract: In the Ecuadorian Amazonia, there is a concern about the presence of high concentrations of cadmium (Cd) in rivers and sediments because of changes in land use and anthropogenic activities, e.g., mining and oil exploitation. Hence, the research related to water treatment processes to meet environmental standards has gained relevance. The use of biochar (BC) as adsorbent is considered a promising and low-cost alternative to improve the water quality in developing countries. In this work, lignocellulosic wastes from *Guadua angustifolia* were transformed through thermochemical treatments, into a promising carbonaceous material, such as BC. BC samples were prepared by pyrolysis (termed pyrochar, PC) and hydrothermal carbonization (termed hydrochar, HC). Their physicochemical properties were correlated with the Cd adsorption removal performance, analyzing the effect of adsorbent dosage, initial solution pH, adsorption kinetics and adsorption isotherms. HC showed the highest Cd adsorption performance, due to the presence of a higher number of oxygenated functional groups, as confirmed by FTIR, XPS and Raman spectroscopy. This research has proposed a sustainable alternative for the recovery of an available waste, contributing to mitigate the effects of the presence of metals on the health and economy of the most vulnerable sectors of society.

Keywords: biochar; *Guadua angustifolia*; pyrolysis; hydrothermal carbonization; cadmium; adsorption



Citation: Navas-Cárdenas, C.; Caetano, M.; Endara, D.; Jiménez, R.; Lozada, A.B.; Manangón, L.E.; Navarrete, A.; Reinoso, C.; Sommer-Márquez, A.E.; Villasana, Y. The Role of Oxygenated Functional Groups on Cadmium Removal using Pyrochar and Hydrochar Derived from *Guadua angustifolia* Residues. *Water* **2023**, *15*, 525. <https://doi.org/10.3390/w15030525>

Academic Editor: Mirna Habuda-Stanic

Received: 6 December 2022

Revised: 13 January 2023

Accepted: 26 January 2023

Published: 28 January 2023



Copyright: © 2023 by the authors. Licensee MDPI, Basel, Switzerland. This article is an open access article distributed under the terms and conditions of the Creative Commons Attribution (CC BY) license (<https://creativecommons.org/licenses/by/4.0/>).

1. Introduction

In South America, especially in Ecuador, the management of mining waste is not adequate, which has promoted heavy metal contamination of several water sources, such as rivers and basins [1]. In the Ecuadorian Amazon Region, the concentration of heavy metals (e.g., cadmium (Cd), arsenic (As), lead (Pb), among others) in some rivers (e.g., Napo and Papallacta rivers) reached values above the permissible limits for the preservation of aquatic life [1–3]. For example, the concentration of Cd (which is one of the most harmful metals that directly affects ecosystems and can have repercussions on human health [4]) in rivers located in the Eastern Andean foothills of the Ecuadorian Amazonia ranges from 3.1 to 46 µg/L, while its permissible limit is 1 µg/L. This fact makes its removal from wastewater prior to discharge into the environment of high importance [5–7].

Several water treatment processes, such as ultrafiltration [8,9], chemical precipitation [10], membrane separation [11], electrochemical deposition [12] and adsorption [5] have been studied to meet environmental standards. Among them, adsorption has attracted a higher interest due to its low-cost and high efficiency [5]. In this sense, biochar (BC) based materials have been considered as promising adsorbents to remove heavy metals (e.g., Cd),

due to their physicochemical properties, such as large surface area, high stability, high amount of surface functional groups and excellent pollutant removal capacity, [13–15]. In a recent study, 72% of Cd was removed using rice husk BC, which exhibited an adsorption capacity of 17.8 mg/g after 120 min adsorption time [16]. Likewise, 90% Cd removal was achieved with a silicate modified oiltea camellia shell-derived BC [17]. Meanwhile, a total Cd removal was reached by using a phosphoric acid-modified HC derived from banana peels as adsorbent [18].

Physicochemical properties, chemical composition and performance of BC strongly depend on the synthesis methods and conditions [19–21]. The thermochemical conversion processes have been the main alternatives to produce BC, where pyrolysis and hydrothermal carbonization (HTC) are the most common pathways. Pyrolysis is a thermochemical conversion of low moisture content waste at high temperature (300–700 °C) in absence of oxygen, used to produce BC, called pyrochar (PC) in this work [22–26]. In contrast, HTC corresponds to a direct thermal conversion of high moisture content waste at low temperatures (180–350 °C) through hydrolysis, dehydration, polymerization and aromatization reactions to obtain a BC product with a high number of functional groups and condensed aromatic structures, termed hydrochar (HC) [27–29]. The physicochemical properties of BC also depend on the residual biomass used as raw material [30–32]. Several residual biomass resources have been studied to produce BC, such as rice husks [16], chicken feather [33], banana [34] and avocado [35] peels, corncob residues [36], wheat straw [37], wood and barks [38,39] and bamboo wastes [40–42].

Guadua angustifolia species represents an endemic bamboo resource in some countries of South America [43]. In Ecuador, 600,000 ha are covered with different types of bamboo, among them, *G. angustifolia* is the most common [44,45]. These materials have been widely used in construction and in the industries producing flooring, panels and agglomerates [46]. However, a large amount of biomass waste is generated by these industries. In fact, only 20 to 30% of the raw material is used and the rest is discarded by the companies [45].

One of the principles of a circular economy is to provide a benefit by using residual biomass. This type of waste can be recycled, reused, refused or renewed to produce energy and other materials, as well as to rethink the way in which they are disposed. In this sense, the use of carbon-based materials obtained from residual biomass (e.g., BC) has attracted great interest due to several applications, such as a solid acid catalyst for biodiesel production [47–51], gas adsorbent [52] and, of course, as adsorbent for contaminant reduction in soil and water [53,54].

Considering these facts and the local availability and cost-effectiveness, this work aims to prepare BC sorbents derived from *G. angustifolia* residues by pyrolysis and HTC and correlate their physicochemical properties with their Cd adsorption efficiency, evaluated as a function of the effect of adsorbent dosage, adsorption kinetics, adsorption isotherms and the initial Cd solution pH. Through this study, it is intended to encourage the circular economy in the Ecuadorian Amazon, based on the exploitation of organic wastes to obtain materials with a potential use for the removal of heavy metals in the waters of the Ecuadorian Amazon Region, by a simple and non-expensive method, such as the adsorption process.

2. Materials and Methods

2.1. Biochar Synthesis and Characterization

G. angustifolia residues were provided by an Ecuadorian bamboo board factory to synthesize both types of biochar: HC and PC. No size reduction operation was performed before the carbonization processes, and the particle size of the residues was very heterogeneous, ranging from some microns to less than 1 cm. Moisture, volatile matter, ash and fixed carbon content were measured according to ASTM-D3173 (Standard Test Method for Moisture in the Analysis Sample of Coal and Coke), ASTM-D3175 (Standard Test Method for Volatile Matter in the Analysis Sample of Coal and Coke) and ASTM-D3174 (Standard Test Method for Ash in the Analysis Sample of Coal and Coke from Coal).

PC was prepared by pyrolysis of biomass residues previously exposed to phosphoric acid. Precisely, 1 kg of guadua residues were immersed in 12 L of 60 wt.% H_3PO_4 aqueous solution at room temperature for 5 h under continuous stirring. After filtering to remove acid excess, the biomass residues were placed in a ceramic crucible, which was introduced into a Nichols-Herreshoff single hearth pilot furnace equipped with a center shaft with a rabble arm for agitation. The pyrolysis was conducted at 550 °C, agitation for 1.5 h, under a reducing environment by setting the fed air/stoichiometric air ratio (λ) to 0.9. After cooling down to room temperature, PC was washed, pH measured, and dried at 90 °C overnight.

HC samples were synthesized by HTC using Teflon-lined stainless steel hydrothermal reactors of 200 mL capacity. This consists of an autoclave, where the pressure is self-generated during the synthesis, due to the heating of the aqueous medium. For this preparation, 5 g of *G. angustifolia* residues were mixed with 80 mL of 50% H_3PO_4 aqueous solution for 3 h. The hydrothermal reactor was hermetically closed and then heated at 200 °C for 5 h in an electric drying oven with a heating rate of 5 °C/min. After natural cooling to ambient temperature, the black biochar composite was filtered and washed several times with distilled water to reach a neutral pH. Finally, the solid sample was dried at 60 °C overnight to obtain HC.

Textural properties of biochar were determined by N_2 adsorption–desorption experiments at 77 K with a Quantachrome Instruments, Nova 4200e (Quantachrome Instruments, Boynton Beach, FL, USA). Before these experiments, all samples were degassed overnight under vacuum at 250 °C. The Brunauer-Emmet-Teller (BET) model was used to determine the specific surface area and the Density Functional Theory (DFT) model was applied to determine the pore size distribution [55]. The Point of Zero Charge (PZC) of HC and PC was determined by the pH drift method [38,56]. Briefly, 0.1 g of each type of biochar was added into a sealed vial with 20 mL of 0.01 M NaCl solution with a pH ranging from 2.0 to 11.0. The initial pH ($\text{pH}_{\text{initial}}$) was adjusted by using 0.1 M HCl and NaOH aqueous solutions. After 24 h of continuous shaking at 200 rpm, the final pH (pH_{final}) of the solution was measured and compared with the $\text{pH}_{\text{initial}}$ value. The PZC of the sample was identified as the value at which pH_{final} is equal to $\text{pH}_{\text{initial}}$.

The surface functional groups in PC and HC were characterized by Fourier Transform Infrared-Attenuated Total Reflectance (FTIR-ATR, Agilent Cary 630) measurements within a wavelength of 400–4000 cm^{-1} . Raman analyses of the samples were conducted on a LabRam HR Evolution Raman spectrometer (Horiba Scientific, Jobin Yvon Technology, Kyoto, Japan) using a laser source with a wavelength of 532 nm, a power of 0.2 mW and a spot size of 5 μm . To determine surface chemical states of biochar components, X-ray Photoelectron Spectroscopy (XPS) analyses were performed on a PHI Versa-Probe III 5000 spectrometer with Al mono $\text{K}\alpha$ X-Ray source at 1486.6 eV under high power mode.

2.2. Cd Adsorption Experiments

All adsorption experiments were performed in a batch mode. To investigate the effect of biochar dosage on Cd removal, a mass of biochar between 25 to 150 mg was added to a beaker containing 50 mL of Cd solution (0.5 mg/L) under a continuous thermostatic oscillation (200 rpm) at 20 °C for 24 h with an orbital shaker. On the other hand, 0.1 M HCl and 0.1 M NaOH solutions were used to study the effect of initial solution pH ($3.0 < \text{pH} < 6.0$), considering a biochar dosage of 2 g/L, an initial Cd concentration of 0.5 mg/L and a shaking time of 3 h (200 rpm).

For the kinetic studies, the contact time varied from 5 to 360 min, at 20 °C, with a biochar dosage of 2 g/L and an initial Cd concentration of 0.5 mg/L. Similar conditions were used for the adsorption equilibrium studies (3 h equilibrium time), in which the Cd initial concentration was evaluated over a range between 0.2 to 1.2 mg/L.

After each Cd adsorption experiment, the suspension was filtered with 0.22 μm PVDF membrane filter. The Cd content in the filtrate was determined by flame atomic absorption

spectroscopy (contrAA 700, Analytik Gena) at 228.8 nm. The Cd removal efficiency (R , %) and adsorption capacity (q_e , mg/g) of each type of biochar were determined [16], as follows:

$$R = \frac{(C_o - C_e)}{C_o} \times 100\% \quad (1)$$

$$q_e = \frac{(C_o - C_e) \times V}{m} \quad (2)$$

where C_o and C_e correspond to the initial concentration and equilibrium concentration of Cd (mg/L), respectively, V is the volume of Cd solution (mL) and m is the mass of biochar (g) used in each experiment.

3. Results and Discussion

3.1. Physicochemical Properties of *G. angustifolia* Residues and Biochar Samples

Proximate analysis results for the biomass residues are shown in Table 1. The high content of volatile matter indicated a composition rich in cellulose and hemicellulose. The fixed carbon content is related to the presence of lignin and is lower than values previously reported in the literature for *G. angustifolia* residues [57]. Pyrolysis yield is affected by the lignin content since this biomass component is difficult to pyrolyze.

Table 1. Physical properties of *G. angustifolia* residues.

Parameter	Content (wt.%)
Moisture	6.4 ± 0.6
Volatile Matter	83.9 ± 2.3
Ash	2.9 ± 0.4
Fixed carbon	13.2 ± 2.2

Textural properties of HC and PC were determined by N₂ adsorption–desorption experiments. As seen in Figure 1, HC biochar presents a composed isotherm (type II and IV) according to the IUPAC classification, with a hysteresis loop H3, that corresponds to solids with no porosity [58], which is in agreement with the low specific surface area determined for the HC biochar (Table 2). HC biochar forms aggregates with a non-rigid texture that generates slit pores of non-uniform size, as observed in the pore size distribution in Figure 1 (insert).

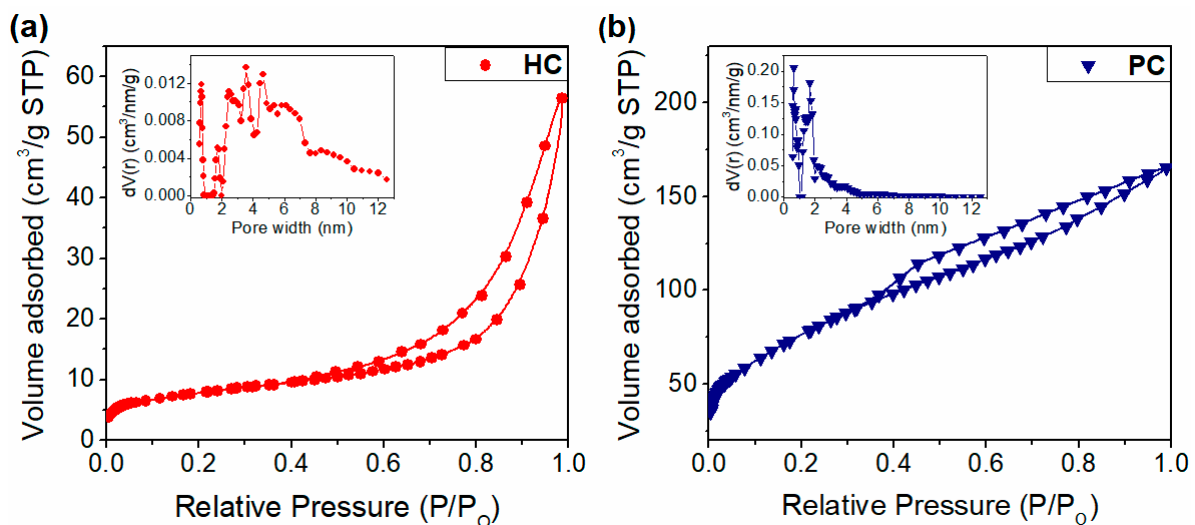


Figure 1. N₂ adsorption–desorption isotherms and DFT pore size distribution (insert) for (a) HC and (b) PC.

Table 2. Textural properties and PZC of HC and PC.

Sample	Specific Surface Area (m ² /g)	Pore Volume (77 K) (cm ³ /g)	Pore Diameter (nm)	PZC
HC	28	0.072	3.5	4.7
PC	238	0.234	0.6	2.6

PC also displays a composed N₂ isotherm (type II and IV) according to the IUPAC classification, with a hysteresis loop H4, often observed for microporous adsorbents having rigidly bound sheets between them [58]. The specific surface area (SSA) determined by the BET model was 238 m²/g, with a pore volume of 0.234 cm³/g (77 K). This result demonstrates that the immersion of the biomass residues in phosphoric acid was effective in obtaining an activated PC biochar. Preliminary PC and HC synthesis experiments were conducted without the use of H₃PO₄, obtaining undetectable SSA values, which confirmed that this acid acts as an activating agent that improves the physicochemical properties of BC-based materials. As phosphoric acid acts as a catalyst for dehydration reactions, the biomass carbonization and porosity are favored by the generation of micropores [59]. Likewise, this type of chemical activation promotes the cleavage of chemical bonds and the intramolecular or intermolecular dehydration of the cellulose or lignocellulose biopolymers and enhances the carbon retention [60,61]. On the other hand, the pore size distribution (PSD) was obtained from applying the DFT model, which provides a more accurate interpretation of the PSD, particularly for microporous materials [62]. These results showed that the PSD is narrow and the pore diameter is below 2 nm, which is consistent with the porosity obtained by phosphoric acid activation [63].

PC has a SSA almost ten times larger than that of HC (Table 2). This is due to the pyrolysis and HTC carbonization processes occurring through specific reactions routes and environments in the reactors, which lead to different textural properties between HC and PC. A larger SSA is supposed to contribute to a better Cd adsorption, however, it is necessary to consider the number and types of functional groups at the surface of each adsorbent, which can further promote the metal removal performance [37,64–66].

PZC plays an important role in the adsorption mechanism [67,68]. This corresponds to the pH at which the material surface has a zero overall electrostatic charge [69–71]. Thus, if the working pH is lower than the PZC of a material, its surface is protonated and positively charged, favoring the electrostatic adsorption of anionic species [72]. On the other hand, its surface can be deprotonated at pH values above its PZC [69,73], which favors the electrostatic adsorption of cationic species.

According to Figure 2, the PZC of PC was 2.6, which indicates that acidic groups were dominant on the biochar surface. This value can be compared to that reported by Wu et al. [74] and Huang et al. [75], who prepared biochar by slow pyrolysis using oak sawdust and *Alternanthera philoxeroides* biomass as feedstock, respectively. Meanwhile, the PZC of HC was 4.7, which is similar to those reported by Nguyen et al. [71], Gai et al. [76], and Saha et al. [77], who prepared biochar samples by pyrolysis and HTC, respectively. These differences in the PZC value have been mainly attributed to the presence of different surface functional groups, as well as their concentration at the surface of each type of biochar [73,77], which, in turn, can depend on the synthesis method and conditions [78–80], modifications with other elements [38,81], and the feedstock [82,83].

As seen in the IR spectra of both types of biochar (Figure 3), HC structure has more functional groups than PC. The IR spectra of HC exhibited a broad peak at 3650–3200 cm^{−1}, which has been attributed to the stretching and deformation vibration of O-H from hydroxyl functional groups generated during the biochar synthesis in an aqueous media [19,84]. Meanwhile, the peak at c.a. 1696 cm^{−1} has been associated with the presence of C=O carbonyl groups [74,85]. Likewise, the peaks at 1593 cm^{−1}, 1428 cm^{−1} and 1201 cm^{−1} in the IR spectrum of HC have been attributed to formation of functional groups associated with the asymmetric stretching vibration of aromatic C=C [84,86], C-O derived from lactone groups [71] and C-O-C stretch of the ethers present in lignin [40,79], respectively. An

additional IR peak at 113 cm^{-1} has been observed in the IR spectra of PC, which has been assigned to the formation of O-P-O bonds, probably generated during the biochar synthesis with phosphoric acid solutions [84,87]. On the other hand, peaks at 1114 cm^{-1} and 799 cm^{-1} were observed only in the HC spectrum, attributed to C-H out-of-plane deformations of the aromatic humic substances generated during HTC of *G. angustifolia* residues [38,74]. The higher presence of C-O, and C=O functional groups on biochar based samples promotes the Cd adsorption behavior of this type of carbonaceous material [27,88]. For instance, Wang et al. [89] prepared biochar based samples by pyrolysis with a lower presence of functional groups compared to those reported by Gargiulo et al. [90] and Pattnaik et al. [40] and Kazak et al. [86], who synthesized biochar based samples by slow pyrolysis and HTC, respectively, with higher adsorption capacities.

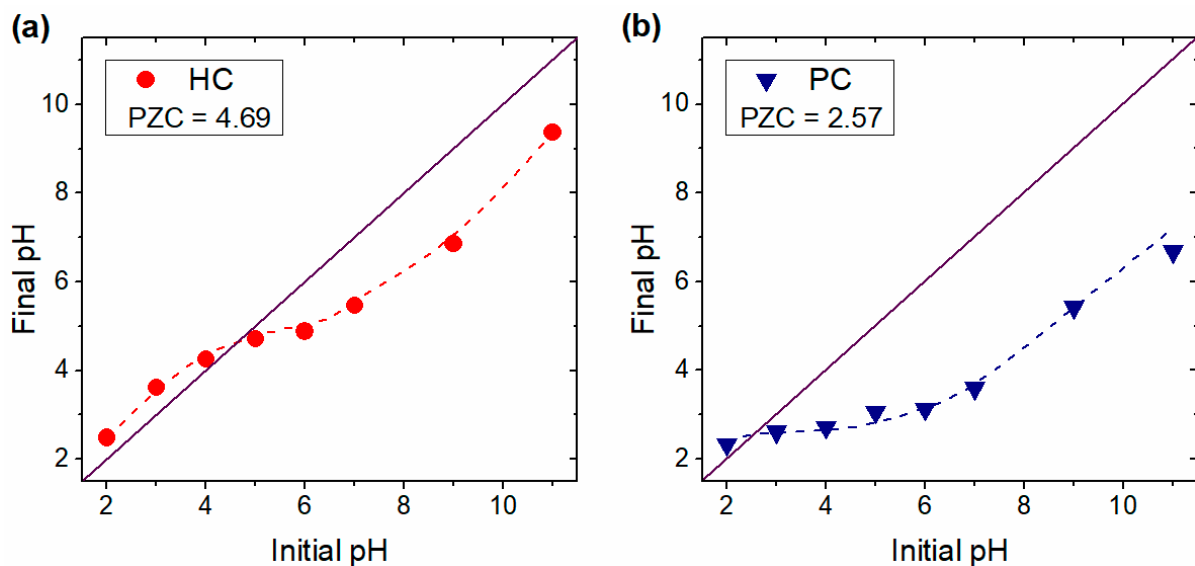


Figure 2. PZC measurement for (a) HC and (b) PC.

The IR results have been corroborated by X-Ray Photoelectron Spectroscopy (XPS). This technique was performed to provide a comparative insight into the bulk material from both HC and PC samples. The XPS spectra indicate the presence of C1s at 284.7 eV and O1s at 532 eV as the key features (Figure 4a) [91]. Fitting processes were developed to identify the chemical environment of both components. Deconvolution analysis of C1s (Figure 4b) showed the presence of functional groups at the surface going from 286.29 eV, 285.72 eV, 286.8 eV, 288.22 eV, that were assigned to C-C, C-O, C=O and O=C-OH, correspondingly shown in Figure 4b [91,92]. Figure 4c shows the high resolution O1's core level spectra of PC and HC, where the fitting unveils four peaks with binding energies at 530.0 eV, 531.58 eV, 532.6 eV, and 534.5 eV that correspond to a carbonyl group, carbonyl oxygen, oxygen carboxylic groups, and oxygen in water, respectively, Figure 4c. The specified binding energy corresponds to each Voigtian equation's peaks and indicates the presence of these types of surface functional groups, in which a given element (C or O) is present on BC and HC surfaces, as seen in the XPS Survey (Figure 4a).

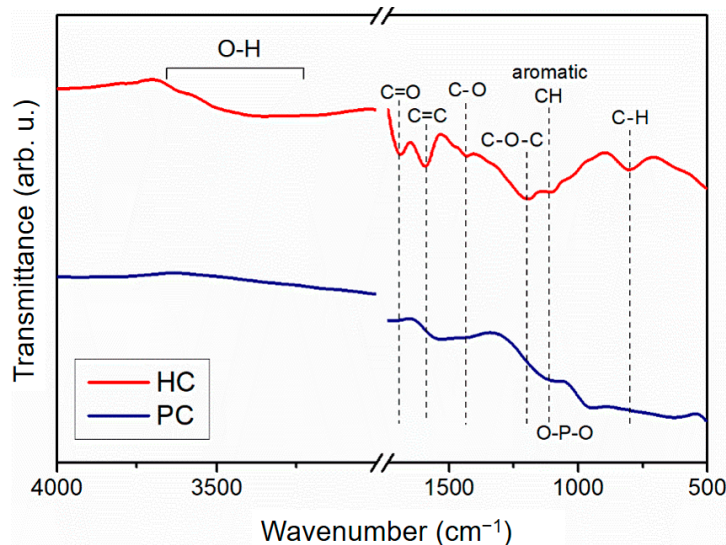


Figure 3. IR spectra of HC and PC.

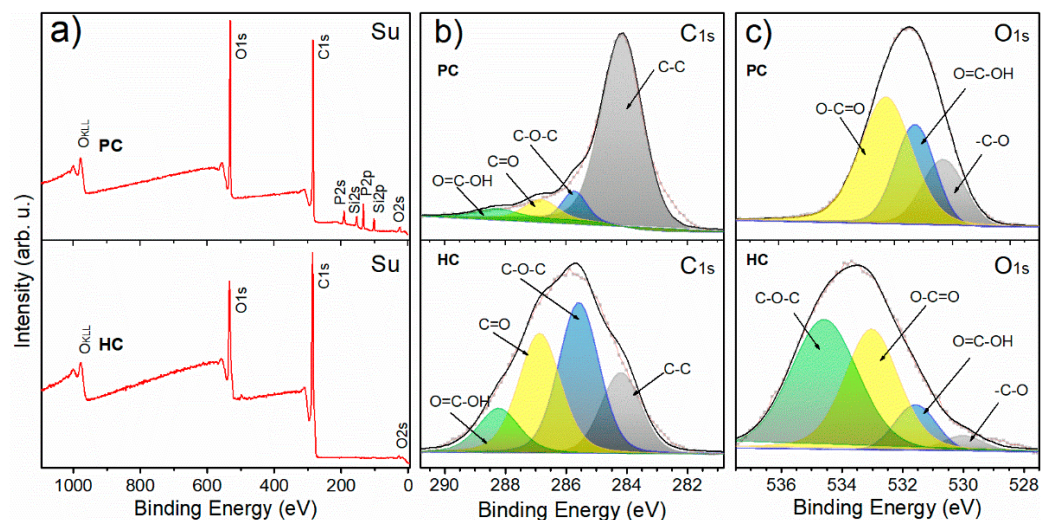


Figure 4. (a) Survey acquisition presenting the atomic concentration, (b) high resolution XPS C1s Core level of PC and HC samples, and (c) deconvolution of O1s.

The fitting area of each contribution on the C1s, shown in Table 3, exhibits the main contribution of C-O-C functional groups for HC and C-C for PC. The large concentration of C-C on PC has been attributed to the presence of graphite groups, which, in turn, indicate a minor generation of oxygenated functional groups at its surface [81,93]. This fact has been confirmed by the O1s core level deconvolution, which presents four instead of three groups on HC compared to PC (see Table 3), confirming the results obtained by IR spectroscopy.

In Raman the spectra of biochar materials shown in Figure 5, it is useful to analyze the D band ($\sim 1350\text{ cm}^{-1}$) which corresponds to low structural orientation, incomplete graphite microcrystals, and structural defects, along with the G band ($\sim 1575\text{ cm}^{-1}$) that corresponds to the stretching vibration of the sp^2 hetero bond in the plane of the carbon network, indicating the ordered graphite-like structure [94,95]. Both, PC and HC present a wide 2D band, ($\sim 2770\text{ cm}^{-1}$) associated with the stacked carbon layers of graphite-like materials [95,96]. Moreover, the crystallinity in the samples was verified by the ratio (I_D/I_G) of the defect intensity peak (~ 1360) and the graphitization intensity peak (~ 1586) [72]. The PC sample presented a better crystallization index of 0.89 with respect to the HC value of 0.94 (Figure 5). The fact that HC has more significant defects means that the graphite-like conjugated π -electron aromatic structures with significant defects, could induce a

π -interaction towards the lone pair of electrons of the metal [96]. Hence, the ability of HC to provide more π -electrons through aromatic and fused rings promotes the adsorption capacity, which was confirmed by FTIR spectra by the presence of the asymmetric stretching vibration of aromatic C=C [97,98].

Table 3. Atomic surface concentration (%) of functional groups on HC and PC obtained from the XPS O1s and C1s core level spectra.

XPS Spectrum	Functional Group	HC		PC	
		BE (eV)	Concentration (%)	BE (eV)	Concentration (%)
O1s	-C-O	530.03	3.61	530.32	20.06
	O=C-OH	531.58	9.75	531.39	28.09
	O-C=O	533.02	38.22	532.60	51.85
	C-O-C	534.59	48.42	-	-
C1s	C-C	284.29	19.43	284.29	85.75
	C-O-C	285.57	36.73	285.72	5.24
	C=O	286.87	31.78	286.83	5.56
	O=C-OH	288.22	12.06	288.15	3.44

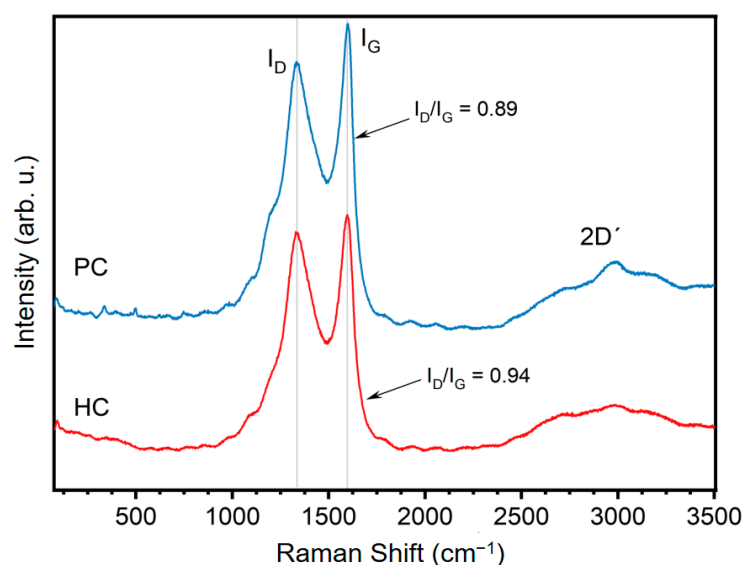


Figure 5. Raman spectra of HC and PC biochar showing its primary features.

3.2. Effect of Biochar Dosage

Biochar dosage is one of the most important factors during the adsorption process, as it determines the adsorbent–adsorbate equilibrium of the system [99]. For this reason, doses of PC and HC ranging from 0.5 to 3 g/L were evaluated in each Cd adsorption experiment using an initial pH of 4.0, which is the pH of the Cd solution of 0.5 mg/L. There is a direct relationship between the HC dosage and Cd removal (red circles, Figure 6). Thus, the lowest Cd removal efficiency (10%) was achieved with a HC dosage of 0.5 g/L, while the highest Cd removal (85%) was reached with 3 g/L of HC. This fact has been attributed to the greater number of adsorption sites accessible for the Cd adsorption process, which is due to the higher availability of more functional groups directly related to the higher mass of adsorbent [37]. A similar behavior of the adsorbent dosage and Cd removal efficiency was reported by Chen et al. [100], who prepared biochar from municipal sewage sludge by pyrolysis (surface area = 67.6 m²/g), in which the Cd removal efficiency increased from 10 to 100% by raising the biochar dosage from 1 g/L to 5 g/L. They, in turn, have also associated the low Cd removal efficiency with the rapid saturation of the limited adsorption

sites used for binding of Cd ions and the high removal efficiency with the presence of a higher amount of new adsorption sites due to the higher mass of adsorbent [100,101].

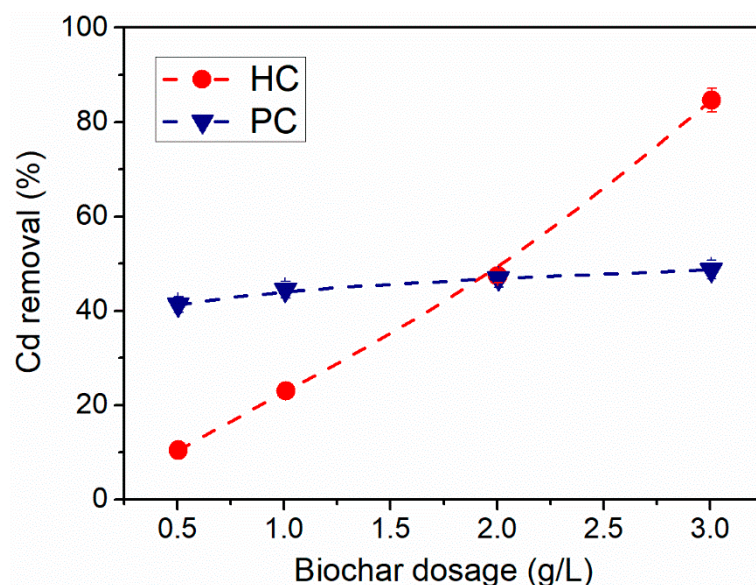


Figure 6. Effect of biochar dosage effect on cadmium removal by HC and PC. Note(s): ($[Cd]_0 = 0.5 \text{ mg/L}$, initial Cd solution pH = 4.0, adsorption time = 24 h).

A considerable effect of the variation of PC dosage on the Cd removal rate (41–48%) was not observed. This can be attributed to the partial or unsuitable use of all biochar adsorption sites or to the formation of aggregates [37,102]. Likewise, a high adsorbent dosage could cause the adsorption performance to remain constant or even decrease [102,103]. During the experiments of Cd adsorption using PC dosages of 2.0 g/L and 3.0 g/L with a 0.5 mg/L Cd solution (initial pH = 4.0), the formation of aggregates was observed, which could explain the reason why the Cd removal rate did not increase as much as in the case of the HC samples. Considering this fact, a higher PC dosage resulted in a greater agglomeration of biochar particles, which, in turn, decreased the number of available adsorption sites and the functional groups for Cd adsorption on this type of carbonaceous material, maintaining the Cd removal values below 50%.

As seen in Figure 6, similar Cd removal rates of PC (46.9%) and HC (47.3%) were obtained using a biochar dosage of 2 g/L under the same adsorption conditions. For this reason and to avoid a greater formation of agglomerates, the kinetic studies and adsorption isotherms were conducted with the aforementioned biochar dosage, although the highest Cd removal was achieved with the highest dose of HC (i.e., 3 g/L).

3.3. Cd Adsorption Kinetics

Figure 7 shows the adsorption capacity of HC and PC as a function of time, for a Cd initial concentration of 0.5 mg/L, at 20 °C, and an adsorbent dosage of 2 g/L. The Cd adsorption capacity of both adsorbents increased with time and then stabilized upon reaching equilibrium (3 h and 1 h for PC and HC, respectively). To confirm this fact, Cd adsorption analyses were performed for 24 h, obtaining similar q_e values to those obtained for the mentioned equilibrium time. Adsorption rates of HC increased from 20 to 44%, when contact time was increased from 5 to 50 min, in contrast to PC, which increased from 20 to 45% at 175 min. HC reached its maximum capacity of adsorption (42%) at 50 min, while PC reached it (47%) at 175 min.

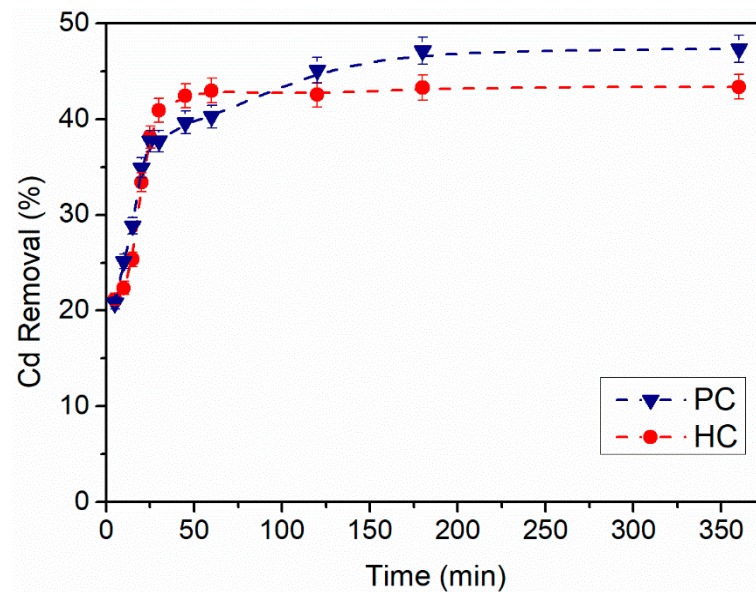


Figure 7. Effect of contact time on cadmium removal by HC and PC. Note(s): (BC dosage = 2 g/L, $[Cd]_0 = 0.5$ mg/L, initial Cd solution pH = 4.0).

The Cd adsorption was rapid on both BC samples in the initial stages (adsorption time below 90 min). These results are comparable to the results reported by Li et al. [104], who evaluated the Cd adsorption performance on rape straw-based BC samples. They indicated that likely adsorption primarily occurs on the outer surfaces of adsorbents. With increasing adsorption time, Cd ions gradually diffuse into the carbon pores and then adsorb onto them [104]. The overall adsorption process is limited by the rate of the adsorption mass transfer steps (i.e., external diffusion, internal diffusion and adsorption on active sites), which, in turn, depend on the adsorbate–adsorbent system and can be evaluated considering its kinetics [105].

For the adsorption kinetic analysis, the experimental data were fitted with the non-linear forms of three standard kinetic models (see Figure 8): pseudo-first order (PFO); pseudo-second order; and Elovich model, since nonlinear forms are appropriate for describing the adsorption kinetics in the liquid phase [106]. The PFO model (3) assumes that the rate of adsorption is related to the number of unoccupied active sites on the adsorbent and it indicates that the adsorption rate is controlled by mass transport (i.e., external diffusion) [107]. The PSO model (4) assumes that the rate of adsorption on the surface of the adsorbent is preceded by internal diffusion and chemisorption [108]. While, the Elovich model (5) describes adsorption processes that follow a chemical adsorption mechanism, considering that the adsorption sites are energetically heterogeneous, so they show different activation energies [109].

Pseudo first order:

$$q_t = Q_e \left(1 - e^{-k_1 t}\right) \quad (3)$$

Pseudo second order:

$$q_t = \frac{k_2 Q_e^2 t}{1 + k_2 Q_e t} \quad (4)$$

Elovich:

$$q_t = \beta \ln(\alpha \beta t) \quad (5)$$

where Q_e (mg/g) is the adsorption capacity of an adsorbent at equilibrium; q_t (mg/g) is the adsorption capacity at time t ; k_1 (1/min) and k_2 (g/mg-min) are the rate constants in the pseudo first and pseudo second order adsorption models, respectively; α is the initial adsorption rate (mg/g-min); β (g/mg) is a constant related to surface coverage and activation energy; and t (min) is the contact time.

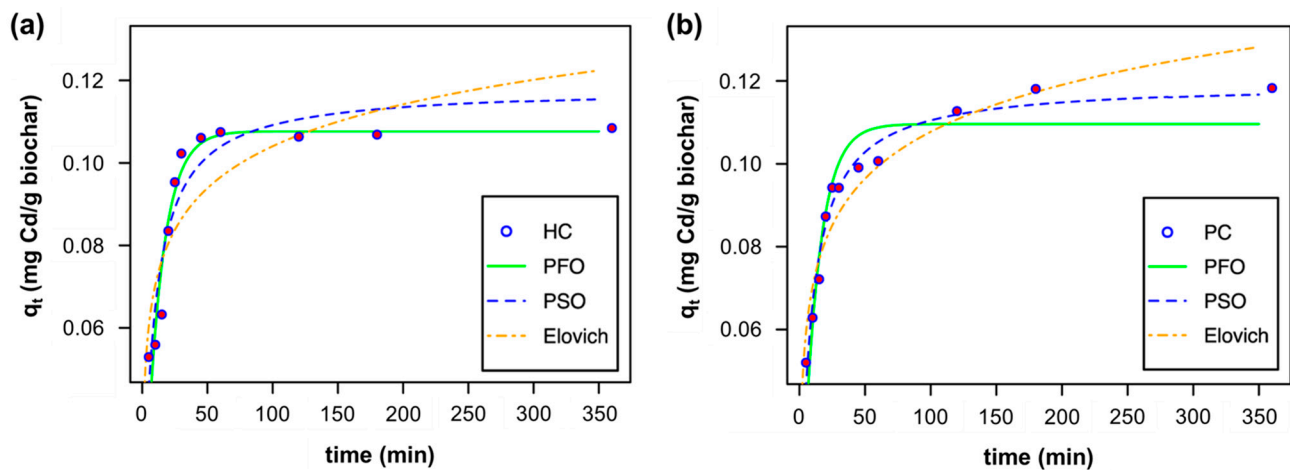


Figure 8. Adsorption Kinetic models of Cd adsorption on (a) HC and (b) PC.

The kinetic models were validated by using the non-linear regression analysis based on the Gauss Newton algorithm, through a script written in R language containing the NLS function. The best-fit model was evaluated in terms of the relative standard error (RSE), which is the ratio between the root mean square error and the standard deviation of the experimental data. Table 4 shows the parameters of the kinetic models evaluated and the RSE for each case (the lowest RSE value is considered to give the best fitting). According to these results and to the fitting shown in Figure 8, the PFO model is the most appropriate to describe the adsorption of Cd onto HC, since its RSE value is the lowest (RSE = 0.0074). Likewise, the $Q_{e,first}$ value is identical to $Q_{e,exp}$ (0.108 mg/g), which suggests that the adsorption is controlled by mass transport (i.e., external diffusion). There is scarce information about the adsorption process of heavy metals on hydrochars that fit the PFO model. However, our results are consistent with the kinetic data reported by Zhu et al., who prepared phosphate-modified activated bamboo BC samples. Likewise, Moussout et al. [110] and Romero-Cano et al. [111] have reported that the PFO model described the adsorption kinetics of Cd onto chitosan-based materials and of Cu on biosorbents prepared from fruit peels, respectively.

Table 4. Parameters for the Pseudo first order, Pseudo second order and Elovich models for Cd adsorption on PC and HC.

Samples	Pseudo First Order			Pseudo Second Order			Elovich			$Q_{e,exp}$ (mg/g)	
	$Q_{e,first}$ (mg/g)	k_1	RSE	$Q_{e,second}$ (mg/g)	k_2	RSE	$Q_{e,elovich}$ (mg/g)	α	β		RSE
HC	0.108	0.080	0.0074	0.118	1.04	0.0083	0.124	0.17	68.13	0.0123	0.108
PC	0.110	0.080	0.0080	0.119	1.04	0.0042	0.119	0.12	61.15	0.0068	0.118

Units of k_1 : (1/min); k_2 : (g/mg-min); α : (mg/g-min); β : (g/mg).

According to Figure 8, the experimental data of adsorption kinetics of Cd on PC better fit the PSO model. Moreover, RSE (0.0042) and Q_e values ($Q_{e,exp} \approx Q_{e,second} = 0.119$ mg/g) confirm the validity of this model, which indicates that the Cd adsorption process is dominated by the chemisorption mechanism, which includes the sharing or exchange of electrons between the adsorbent and adsorbate as covalent forces, and ion exchange [107]. These results are in agreement with those reported by Saeed et al. [112], who determined that chemisorption was associated with the Cd adsorption process on kenaf fiber-derived PC. Moreover, similar results were reported by Wang et al. [106] who studied BC samples from willow wood and cattle manure prepared by pyrolysis. In addition, calculated Q_e values from the Elovich model is near to $Q_{e,exp}$ (see Table 4). These results corroborate that

the Cd adsorption on PC is determined by the chemisorption, since the two aforementioned models (PSO and Elovich) are based on this mechanism.

3.4. Adsorption Isotherms

Adsorption isotherms correlate the Cd adsorption capacity for each adsorbent (q_e) and the Cd concentration in the solution at equilibrium (C_e) [113], and are shown in Figure 9. To analyze the Cd adsorption behavior on HC and PC, Langmuir [114], Freundlich [115] and Temkin [116] models were considered, in which the non-linear least squares estimates of the parameters were obtained through a script written in R language containing the NLS function, which uses the Gauss Newton algorithm.

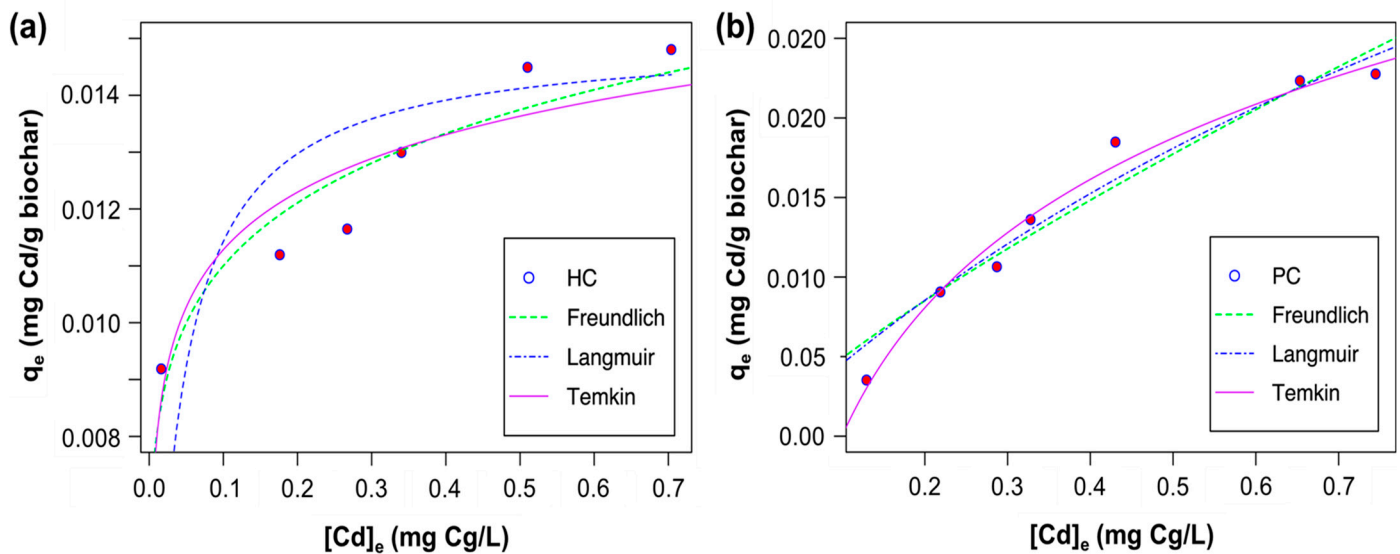


Figure 9. Adsorption isotherms for (a) HC and (b) PC.

Langmuir proposed that all metal ions are chemically adsorbed to a fixed number of free sites, which are energetically equivalent [114]. The linear form of his theory, relates the ratio of the adsorbate solution concentration and the adsorbed concentration at equilibrium, C_e/q_e , to adsorption capacity q_{max} [117]:

Langmuir:

$$\frac{C_e}{q_e} = \frac{1}{b \cdot q_{max}} + \frac{C_e}{q_{max}} \tag{6}$$

where b is the adsorption constant.

In contrast, Freundlich associated the mass of metal adsorbed by unit mass, q_e (mg/g), with the concentration of a solute adsorbed onto the surface of a solid:

Freundlich:

$$\log(q_e) = \log(K_f) + \frac{1}{n} \log(C_e) \tag{7}$$

where K_f and $1/n$ are constants that indicate the adsorption capacity for a given adsorbate and adsorbent at a given temperature.

Temkin assumes that the concentration of adsorbate adsorbed at equilibrium (mg/g), q_e , is proportional to the sum of the log of the Temkin isotherm constant, A (L/g), and the log of adsorbate concentration in solution at equilibrium, C_e (mg/L):

Temkin:

$$q_e = B \ln(A) + B \ln(C_e) \tag{8}$$

where B is equal to RT/b and represents the heat of adsorption and A is the Temkin constant (J/mol).

HC data for adsorption experiments followed the model of the Langmuir isotherm (RSE = 0.0070), suggesting that all adsorption sites are energetically equivalent, and the

uptake of Cd occurs by monolayer adsorption without interactions between metal ions adsorbed by active sites of the adsorbent [118]. PC was best modelled by the Temkin isotherm model (RSE = 0.0108), indicating that the adsorption heat of all molecules decreases linearly with the surface coverage of the adsorbent and the adsorption process is distinguished by a uniform distribution of binding energies (see Figure 9 and Table 5) [119]. Moreover, in the Freundlich isotherm model, the value of n was calculated as 7.95 and 0.97 for HC and PC, respectively, which suggests that the Cd adsorption occurred physically and desirably on the PC surface [118].

Table 5. Langmuir, Freundlich and Temkin constants for Cd adsorption isotherms on HC and PC.

Sample	Freundlich			Langmuir			Temkin		
	n	K_F (mg/g)	RSE	q_m (mg/g)	Q_L (L/mg)	RSE	A_T (L/mg)	B_T (J/mg)	RSE
HC	7.95	0.15	0.0075	0.16	18.56	0.0070	22.64	0.015	0.0093
PC	0.97	0.37	0.0198	0.59	0.90	0.0165	10.00	0.116	0.0108

According to the experimental results, the maximum Cd adsorption was 0.14 and 0.22 mg Cd/g for HC and PC, respectively. Although these values are lower than those reported with other adsorbents [5,33,39], they are similar than those reported by Mohan et al. [120], who prepared BC-based materials derived from pine bark and oak wood obtaining Cd adsorption values ranging from 0.34 to 0.37 mg Cd/g. Furthermore, for a better understanding of the performance of these materials during the removal of Cd in water, the normalized maximum adsorption capacities with the specific surface area were calculated from experimental and calculated terms of the isotherms (Table 6). Results confirmed that the difference in the performance of HC and PC in the removal of Cd from water is promoted by the presence of more functional groups in HC with respect to PC, as described with FTIR and confirmed by Raman and XPS. Although the Freundlich adsorption model is not suitable to accurately determine the absolute maximum adsorption value, it is useful for analyzing the adsorption maximum of both materials. It is evident that, despite its low SSA, the HC is more efficient at removing Cd than PC.

Table 6. Surface area normalized adsorption maximum values of Cd adsorption for HC and PC.

Sample	q_e/SSA^a $\mu\text{g}/\text{m}^2$	q_{max}/SSA^b $\mu\text{g}/\text{m}^2$	K_f/SSA^c $\mu\text{g}/\text{m}^2$
HC	5.14	5.71	5.32
PC	0.92	0.003	1.55

Note: SSA: Specific surface area. ^a Experimental adsorption maximum values of Cd with $[Cd]_0 = 0.8$ mg/L. ^b Maximum adsorption capacity calculated from the Langmuir isotherm. ^c Freundlich constant related to SSA.

3.5. Effect of Solution Initial pH

The solution initial pH is one of the main factors to be considered during the study of Cd adsorption on BC samples. It is important to indicate that the pH of real water bodies, located in areas where adsorption treatment can be conducted (e.g., waters containing Cd from the rivers at the Ecuadorian Amazon Region) has values ranging from 5.2 to 7.0 [121,122], so it is necessary to regulate this operating condition for the adsorption process. Cd removal obtained with PC and HC strongly depended on the initial pH of the Cd aqueous solution, which ranged from 2.0 to 6.0. Initial solution pH values above 6.0 were not evaluated in order to avoid Cd precipitation and to further study its adsorption on the carbonaceous materials [39].

As seen in Figure 10, the lowest removal and adsorption capacity of Cd on PC and HC were obtained at an initial pH of 2.0. These performances have been attributed to the PZC of each adsorbent. As seen in Table 2 and Figure 2, the PZC of PC and HC were 2.6 and 4.7, respectively. Considering this fact, the surface of each type of BC was protonated at pH conditions below their PZC, which could favor the adsorption of anionic species [27,68,123].

However, Cd cations experienced electrostatic repulsion with the positively charged BC surface, inhibiting the metal adsorption [36,39]. The same behavior was observed during the Cd adsorption on HC at pH 3.0 (Cd removal below 5%), which was also a condition in which the Cd cations were electrostatically repulsed from the BC surface [37]. This fact has also been reported by Den et al. [124], who prepared corncob-based biochars obtaining Cd removal values below 10% at acidic conditions (pH < 4.0). These authors, in turn, have associated the poor removal efficiency to the higher concentration of H⁺ in water, which generates a competitive sorption between them and metal ions, in addition to the adsorbent–adsorbate electrostatic repulsion.

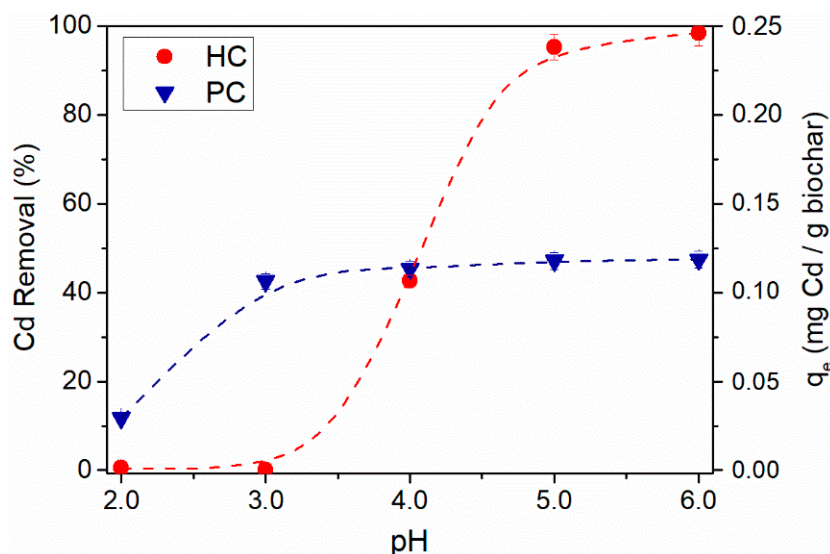


Figure 10. Effect of solution initial pH on Cd removal by HC and PC.

In the Cd adsorption experiments with PC, by raising the initial solution pH up to values above 4.0, the Cd removal increased from 11.7% to 47.1%. This has been mainly associated with the PZC of PC, which was 2.7. Thus, at pH values above its PZC, the PC surface was deprotonated, favoring the Cd adsorption on the positively charged surface. This fact also explains the Cd adsorption behavior obtained with HC, in which the Cd removal increased from 0 to 100% by raising the initial pH up to values above 5.0. This behavior has been also reported by several authors [33,74,78,125], who have associated it to the negatively charged BC surface generated due to the ionization or dissociation of oxygen functional groups (e.g., carboxyl, hydroxyl and phenolic groups).

The highest Cd removals (and the highest Cd adsorption capacities) for HC and PC were obtained during the adsorption experiments conducted at initial pH values above 5.0 (Figure 10). Furthermore, it is important to note that, at these pH conditions, the Cd adsorption performance with HC was greater than that of PC. Particularly, the Cd adsorption capacity of HC and PC, after 3 h of shaking time with an initial Cd concentration of 0.5 mg/L (initial solution pH = 5.0 and 6.0), were 0.25 and 0.12 mg Cd/g, respectively, which correspond to metal adsorption capacities normalized by SSA of 8.87 and 0.503 $\mu\text{g}/\text{m}^2$. This behavior has been attributed to the higher number of functional groups at the HC surface (as reported in the IR, XPS and Raman spectra, Figures 3–5), despite its SSA being lower than that of PC (Table 2). In this sense, one can suggest that the HTC synthesis is a suitable alternative to produce carbonaceous materials with a high number of functional groups that can promote the Cd adsorption (e.g., HC). This fact, in turn, meets the circular economy principles, especially in zones with high production of residual biomass derived from *G. angustifolia*, providing a low-cost and effective way to reuse them in order to obtain sorbents for heavy metals, like Cd.

3.6. Cost Analysis of HC and PC Preparation

The cost analysis plays a vital role in determining the feasibility of the production process of HC and PC and the execution of cost-effective water treatment. The availability and collection of raw material, treatment conditions, carbonization, washing, drying and reuse have been considered the most critical cost-influencing factors for this analysis [126,127]. The generation of a large amount of *G. angustifolia* residues from the Ecuadorian bamboo industries exhibits the accessibility of this raw material for BC production at a large scale. Considering these facts, Table 7 summarizes the cost estimation analysis to produce 1 kg of HC and PC, in dollars (USD).

Table 7. Estimated cost analysis for the production of HC and PC.

Particulars	Sub Sections	Cost Break Up	Total Cost (USD)	
			HC	PC
Raw material processing	Collection or purchase of raw material cost	Collected from local companies with free of cost	0.00	0.00
	Drying	Sunlight drying hours \times units \times cost per max heat level	0.00	0.00
Biochar preparation	HTC/Pyrolysis cost	HTC cost = $5 \times 1 \times 0.11$	0.55	0.44
		Pyrolysis cost = $1.5 \times 1 \times 0.29$		
	Washing cost	material was cleaned by distilled water: hours \times units \times per unit cost = $1 \times 1 \times 0.054$	0.05	0.05
	Drying cost	hours \times unit \times per unit cost = $12 \times 1 \times 0.054$	0.65	0.65
Net cost	Cost of H ₃ PO ₄		1.71	1.71
10% overall cost			2.96	2.85
Total cost			3.26	3.14

According to this analysis, the estimated cost to produce 1 kg of HC and PC from *G. angustifolia* residues is \$3.26 and \$3.14, respectively. Their production cost is more expensive than other types of BC prepared at larger scale (\$0.90–\$2.78) [128–130], which is mainly due to the cost incurred using H₃PO₄ as BC activator (see Table 7). In this work, H₃PO₄ was necessary to improve the BC physicochemical properties (e.g., SSA, pore volume and number of functional groups) and its Cd adsorption capacity. Preliminary studies were conducted using HC and PC samples prepared without H₃PO₄, obtaining undetectable SSA and Cd removal values. Moreover, it has been widely reported that the use of H₃PO₄ as BC activator results in a better porous structure [33,59,60,131]. Likewise, this promotes the carbon retention during the BC synthesis, generating some C-O-P-like complexes on its surface, which, in turn, enhance its thermal stability [59,132,133]. In addition, H₃PO₄ can be easily recovered after washing the sample and it can be reused for the activation of other carbonaceous materials [134,135].

The production cost of HC and PC is comparable to that of BC samples derived from teff straw and activated with H₃PO₄ with similar concentration, whose cost ranges from \$2.80 (for HC) to \$3.35 (for PC) [136]. Moreover, the cost incurred to produce HC and PC using Ecuadorian *G. angustifolia* residues is lower than that of BC derived from sugarcane bagasse activated with 85 wt.% H₃PO₄ concentrated solution (i.e., \$3.64) [137], which may cause a harmful effect on environmental safety if a process of reuse or recovery of this activating agent is not considered. On the other hand, although the Cd adsorption capacities of HC and PC are lower than that reported for other BC derived from bamboo wastes ($q = 24.8 - 28.9$ mg Cd/g) [42], the production of this type of carbonaceous materials could be viable, considering that Ecuadorian bamboo industries do not have an adequate management of guadua residues, which are 80% or more as previously described. Hence, this type of by-product can be used as raw material to produce an adsorbent, generating added value and promoting a circular economy in the region. Its application can be a simple and cost-effective alternative to treat water containing heavy metals (e.g., Cd). Finally, it should be noted that this technology is still under development in South America and this

study can serve as a guide for future large-scale applications of BC, giving the opportunity to promote bioeconomy in sectors where water quality is very poor.

4. Conclusions

In this study, two types of BC were prepared by pyrolysis and HTC using *G. angustifolia* residues provided by an Ecuadorian bamboo board factory. The physicochemical properties of HC and PC were evaluated by several techniques. Using porosimetry, IR, XPS, and Raman spectroscopy, it was possible to determine SSA for each BC as well as the presence of different functional groups at their surface. Cd adsorption studies were performed by varying the sorbent dosage, adsorption time, initial Cd concentration and initial solution pH. Cd adsorption kinetics were described by a pseudo-first order and pseudo-second order kinetic rate expressions for HC and PC, respectively, suggesting that the external diffusion and chemisorption are the mechanisms of Cd adsorption for each case. Likewise, the Cd adsorption results for HC and PC were correlated with the Langmuir and Temkin isotherms, respectively. Considering the experimental results, the equilibrium Cd adsorption capacities of both types of BC were determined and then normalized in terms of their SSA, which were 5.14 and 0.92 $\mu\text{g Cd/m}^2$ for HC and PC, respectively, which are, in turn, similar to that previously reported for BC adsorbents derived from other bamboo wastes. By varying the initial Cd solution pH, 100% Cd removal was achieved by using HC as sorbent, with an initial solution pH above 5.0, a BC dosage of 2 g/L and adsorption time of 3 h. Meanwhile with PC, the highest Cd removal was near 50%. The higher Cd adsorption performance obtained with HC was associated with a higher presence of oxygenated functional groups at its surface, despite its low SSA compared to that of PC. Finally, an estimated cost analysis was performed, obtaining similar costs of production of HC (\$3.26/kg) and PC (\$3.14/kg), which are similar and even a bit cheaper than other BC materials activated with H_3PO_4 . These results indicate that HTC is an appropriate alternative to produce carbonaceous materials derived from *G. angustifolia* residues to be used to treat waters containing Cd, promoting the circular economy principles in South American regions.

Author Contributions: Conceptualization, C.N.-C., Y.V. and D.E.; methodology, C.N.-C., Y.V., D.E., A.E.S.-M., L.E.M., C.R., A.B.L. and A.N.; validation, A.E.S.-M., C.N.-C. and Y.V.; formal analysis, C.N.-C., Y.V., M.C., A.E.S.-M., D.E., L.E.M., C.R. and R.J.; investigation, C.N.-C., Y.V., R.J., C.R. and D.E.; resources, C.N.-C., Y.V., C.R., M.C. and D.E.; data curation, C.N.-C., Y.V., C.R., L.E.M., D.E., M.C. and R.J.; writing—original draft preparation, C.N.-C., Y.V., D.E., A.E.S.-M., L.E.M., C.R., R.J., A.B.L. and A.N.; writing—review and editing, C.N.-C., Y.V., A.E.S.-M., D.E., M.C. and L.E.M.; visualization, C.N.-C., M.C. and C.R.; supervision, C.N.-C.; project administration, C.N.-C.; funding acquisition, C.N.-C., Y.V. and D.E. All authors have read and agreed to the published version of the manuscript.

Funding: This research and the APC were funded by the Ecuadorian Corporation for the Development of Research and the Academy (CEDIA), project number CEPRA XVI-2022-13 BioFe.

Data Availability Statement: Not applicable.

Acknowledgments: The authors would like to thank the financial support of the Ecuadorian Corporation for the Development of Research and the Academy (CEDIA) in the development of this study, within the Project Grant CEPRA XVI-2022-13 BioFe.

Conflicts of Interest: The authors declare no conflict of interest.

References

1. Capparelli, M.V.; Cabrera, M.; Rico, A.; Lucas-Solis, O.; Alvear, S.D.; Vasco, S.; Galarza, E.; Shiguango, L.; Pinos-Velez, V.; Pérez-González, A.; et al. An Integrative Approach to Assess the Environmental Impacts of Gold Mining Contamination in the Amazon. *Toxics* **2021**, *9*, 149. [[CrossRef](#)]
2. Capparelli, M.V.; Moulatlet, G.M.; de Abessa, D.M.S.; Lucas-Solis, O.; Rosero, B.; Galarza, E.; Tuba, D.; Carpintero, N.; Ochoa-Herrera, V.; Cipriani-Avila, I. An Integrative Approach to Identify the Impacts of Multiple Metal Contamination Sources on the Eastern Andean Foothills of the Ecuadorian Amazonia. *Sci. Total Environ.* **2020**, *709*, 136088. [[CrossRef](#)] [[PubMed](#)]
3. Cumbal, L.H.; Bundschuh, J.; Aguirre, V.; Murgueitio, E.; Tipán, I.; Chavez, C. *The Origin of Arsenic in Waters and Sediments from Papallacta Lake Area in Ecuador*; Taylor & Francis: Abingdon-on-Thames, UK, 2009.

4. Jiménez-Oyola, S.; García-Martínez, M.J.; Ortega, M.F.; Chavez, E.; Romero, P.; García-Garizabal, I.; Bolonio, D. Ecological and Probabilistic Human Health Risk Assessment of Heavy Metal(Loid)s in River Sediments Affected by Mining Activities in Ecuador. *Environ. Geochem. Health* **2021**, *43*, 4459–4474. [[CrossRef](#)] [[PubMed](#)]
5. Pyrzynska, K. Removal of Cadmium from Wastewaters with Low-Cost Adsorbents. *J. Environ. Chem. Eng.* **2019**, *7*, 40. [[CrossRef](#)]
6. World Health Organization. *Guidelines for Drinking-Water Quality*; WHO Library: Geneva, Switzerland, 2017; ISBN 9789241549950.
7. Li, C.; Zhou, K.; Qin, W.; Tian, C.; Qi, M.; Yan, X.; Han, W. A Review on Heavy Metals Contamination in Soil: Effects, Sources, and Remediation Techniques. *Soil Sediment Contam.* **2019**, *28*, 380–394. [[CrossRef](#)]
8. Carolin, C.F.; Kumar, P.S.; Saravanan, A.; Joshiba, G.J.; Naushad, M. Efficient Techniques for the Removal of Toxic Heavy Metals from Aquatic Environment: A Review. *J. Environ. Chem. Eng.* **2017**, *5*, 2782–2799. [[CrossRef](#)]
9. Jellouli Ennigrou, D.; Gzara, L.; Ramzi Ben Romdhane, M.; Dhahbi, M. Cadmium Removal from Aqueous Solutions by Polyelectrolyte Enhanced Ultrafiltration. *Desalination* **2009**, *246*, 363–369. [[CrossRef](#)]
10. Islamoglu, S.; Yilmaz, L.; Ozbelge, H.O. Development of a Precipitation Based Separation Scheme for Selective Removal and Recovery of Heavy Metals from Cadmium Rich Electroplating Industry Effluents. *Sep. Sci. Technol.* **2006**, *41*, 3367–3385. [[CrossRef](#)]
11. Qdais, H.A.; Moussa, H. Removal of Heavy Metals from Wastewater by Membrane Processes: A Comparative Study. *Desalination* **2004**, *164*, 105–110. [[CrossRef](#)]
12. Wang, Y.; Xu, W.; Zhuo, Q.; Xu, Z.; Guo, Q. Electrochemical Recovery of Metals from Cadmium Wastewater. *Chem. Lett.* **2014**, *43*, 1312–1314. [[CrossRef](#)]
13. Dai, Y.; Zhang, N.; Xing, C.; Cui, Q.; Sun, Q. The Adsorption, Regeneration and Engineering Applications of Biochar for Removal Organic Pollutants: A Review. *Chemosphere* **2019**, *223*, 12–27. [[CrossRef](#)]
14. He, P.; Zhang, H.; Duan, H.; Shao, L.; Lü, F. Continuity of Biochar-Associated Biofilm in Anaerobic Digestion. *Chem. Eng. J.* **2020**, *390*, 124605. [[CrossRef](#)]
15. Álvarez, M.L.; Gascó, G.; Palacios, T.; Paz-Ferreiro, J.; Méndez, A. Fe Oxides-Biochar Composites Produced by Hydrothermal Carbonization and Pyrolysis of Biomass Waste. *J. Anal. Appl. Pyrolysis* **2020**, *151*, 104893. [[CrossRef](#)]
16. Ameen Hezam Saeed, A.; Yub Harun, N.; Mahmoud Nasef, M.; Al-Fakih, A.; Abdulhakim Saeed Ghaleb, A.; Kolawole Afolabi, H. Removal of Cadmium from Aqueous Solution by Optimized Rice Husk Biochar Using Response Surface Methodology. *Ain Shams Eng. J.* **2022**, *13*, 101516. [[CrossRef](#)]
17. Cai, T.; Liu, X.; Zhang, J.; Tie, B.; Lei, M.; Wei, X.; Peng, O.; Du, H. Silicate-Modified Oiltea Camellia Shell-Derived Biochar: A Novel and Cost-Effective Sorbent for Cadmium Removal. *J. Clean. Prod.* **2021**, *281*, 125390. [[CrossRef](#)]
18. Ge, Q.; Tian, Q.; Wang, S.; Zhang, J.; Hou, R. Highly Efficient Removal of Lead/Cadmium by Phosphoric Acid-Modified Hydrochar Prepared from Fresh Banana Peels: Adsorption Mechanisms and Environmental Application. *Langmuir* **2022**; *in press*. [[CrossRef](#)] [[PubMed](#)]
19. Luo, M.; Lin, H.; He, Y.; Li, B.; Dong, Y.; Wang, L. Efficient Simultaneous Removal of Cadmium and Arsenic in Aqueous Solution by Titanium-Modified Ultrasonic Biochar. *Bioresour. Technol.* **2019**, *284*, 333–339. [[CrossRef](#)]
20. Cha, J.S.; Park, S.H.; Jung, S.C.; Ryu, C.; Jeon, J.K.; Shin, M.C.; Park, Y.K. Production and Utilization of Biochar: A Review. *J. Ind. Eng. Chem.* **2016**, *40*, 1–15. [[CrossRef](#)]
21. Wang, J.; Wang, S. Preparation, Modification and Environmental Application of Biochar: A Review. *J. Clean. Prod.* **2019**, *227*, 1002–1022. [[CrossRef](#)]
22. Salgado, M.A.H.; Tarelho, L.A.C.; Matos, A. Analysis of Combined Biochar and Torrefied Biomass Fuel Production as Alternative for Residual Biomass Valorization Generated in Small-Scale Palm Oil Mills. *Waste Biomass Valoriz.* **2020**, *11*, 343–356. [[CrossRef](#)]
23. Glaser, B.; Parr, M.; Braun, C.; Kopoló, G. Biochar Is Carbon Negative. *Nat. Geosci.* **2009**, *2*, 2. [[CrossRef](#)]
24. Liu, Z.; Han, G. Production of Solid Fuel Biochar from Waste Biomass by Low Temperature Pyrolysis. *Fuel* **2015**, *158*, 159–165. [[CrossRef](#)]
25. Roberts, K.G.; Gloy, B.A.; Joseph, S.; Scott, N.R.; Lehmann, J. Life Cycle Assessment of Biochar Systems: Estimating the Energetic, Economic, and Climate Change Potential. *Environ. Sci. Technol.* **2010**, *44*, 827–833. [[CrossRef](#)] [[PubMed](#)]
26. Rashidi, N.; Yausup, S. A Mini Review of Biochar Synthesis, Characterization, and Related Standardization and Legislation. In *Applications of Biochar for Environmental Safety*; IntechOpen: London, UK, 2020.
27. Liu, Z.; Wang, Z.; Chen, H.; Cai, T.; Liu, Z. *Hydrochar and Pyrochar for Sorption of Pollutants in Wastewater and Exhaust Gas: A Critical Review*; Elsevier Ltd.: Amsterdam, The Netherlands, 2021; Volume 268, ISBN 8610627373.
28. Mäkelä, M.; Benavente, V.; Fullana, A. Hydrothermal Carbonization of Lignocellulosic Biomass: Effect of Process Conditions on Hydrochar Properties. *Appl. Energy* **2015**, *155*, 576–584. [[CrossRef](#)]
29. Donar, Y.O.; Çağlar, E.; Sinağ, A. Preparation and Characterization of Agricultural Waste Biomass Based Hydrochars. *Fuel* **2016**, *183*, 366–372. [[CrossRef](#)]
30. Kamali, M.; Appels, L.; Kwon, E.E.; Aminabhavi, T.M.; Dewil, R. Biochar in Water and Wastewater Treatment—A Sustainability Assessment. *Chem. Eng. J.* **2021**, *420*, 129946. [[CrossRef](#)]
31. Hagemann, N.; Spokas, K.; Schmidt, H.P.; Kägi, R.; Böhler, M.A.; Bucheli, T.D. Activated Carbon, Biochar and Charcoal: Linkages and Synergies across Pyrogenic Carbon’s ABCs. *Water* **2018**, *10*, 182. [[CrossRef](#)]
32. Srivatsav, P.; Bhargav, B.S.; Shanmugasundaram, V.; Arun, J.; Gopinath, K.P.; Bhatnagar, A. Biochar as an Eco-Friendly and Economical Adsorbent for the Removal of Colorants (Dyes) from Aqueous Environment: A Review. *Water* **2020**, *12*, 3561. [[CrossRef](#)]

33. Chen, H.; Li, W.; Wang, J.; Xu, H.; Liu, Y.; Zhang, Z.; Li, Y.; Zhang, Y. Adsorption of Cadmium and Lead Ions by Phosphoric Acid-Modified Biochar Generated from Chicken Feather: Selective Adsorption and Influence of Dissolved Organic Matter. *Bioresour. Technol.* **2019**, *292*, 121948. [[CrossRef](#)]
34. Amin, M.T.; Alazba, A.A.; Shafiq, M. Removal of Copper and Lead Using Banana Biochar in Batch Adsorption Systems: Isotherms and Kinetic Studies. *Arab. J. Sci. Eng.* **2018**, *43*, 5711–5722. [[CrossRef](#)]
35. Prabakaran, E.; Pillay, K.; Brink, H. Hydrothermal Synthesis of Magnetic-Biochar Nanocomposite Derived from Avocado Peel and Its Performance as an Adsorbent for the Removal of Methylene Blue from Wastewater. *Mater. Today Sustain.* **2022**, *18*, 100123. [[CrossRef](#)]
36. Luo, M.; Lin, H.; Li, B.; Dong, Y.; He, Y.; Wang, L. A Novel Modification of Lignin on Corn-cob-Based Biochar to Enhance Removal of Cadmium from Water. *Bioresour. Technol.* **2018**, *259*, 312–318. [[CrossRef](#)] [[PubMed](#)]
37. Naeem, M.A.; Imran, M.; Amjad, M.; Abbas, G.; Tahir, M.; Murtaza, B.; Zakir, A.; Shahid, M.; Bulgariu, L.; Ahmad, I. Batch and Column Scale Removal of Cadmium from Water Using Raw and Acid Activated Wheat Straw Biochar. *Water* **2019**, *11*, 1438. [[CrossRef](#)]
38. Arbelaez Breton, L.; Mahdi, Z.; Pratt, C.; El Hanandeh, A. Modification of Hardwood Derived Biochar to Improve Phosphorus Adsorption. *Environments* **2021**, *8*, 41. [[CrossRef](#)]
39. Mohan, D.; Kumar, H.; Sarswat, A.; Alexandre-Franco, M.; Pittman, C.U. Cadmium and Lead Remediation Using Magnetic Oak Wood and Oak Bark Fast Pyrolysis Biochars. *Chem. Eng. J.* **2014**, *236*, 513–528. [[CrossRef](#)]
40. Pattnaik, D.; Kumar, S.; Bhuyan, S.K.; Mishra, S.C. Effect of Carbonization Temperatures on Biochar Formation of Bamboo Leaves. *IOP Conf. Ser. Mater. Sci. Eng.* **2018**, *338*, 54. [[CrossRef](#)]
41. Alchouron, J.; Navarathna, C.; Chludil, H.D.; Dewage, N.B.; Perez, F.; Hassan, E.B.; Pittman, C.U.; Vega, A.S.; Mlsna, T.E. *Assessing South American Guadua Chacoensis Bamboo Biochar and Fe₃O₄ Nanoparticle Dispersed Analogues for Aqueous Arsenic(V) Remediation*; Elsevier: Amsterdam, The Netherlands, 2020; Volume 706, ISBN 6623251618.
42. Zhang, S.; Zhang, H.; Cai, J.; Zhang, X.; Zhang, J.; Shao, J. Evaluation and Prediction of Cadmium Removal from Aqueous Solution by Phosphate-Modified Activated Bamboo Biochar. *Energy Fuels* **2018**, *32*, 4469–4477. [[CrossRef](#)]
43. Olivier, J.; Otto, T.; Roddaz, M.; Antoine, P.O.; Londoño, X.; Clark, L.G. First Macrofossil Evidence of a Pre-Holocene Thorny Bamboo Cf. *Guadua* (Poaceae: Bambusoideae: Bambuseae: Guaduiniae) in South-Western Amazonia (Madre de Dios—Peru). *Rev. Palaeobot. Palynol.* **2009**, *153*, 1–7. [[CrossRef](#)]
44. Ministry of Agriculture and Livestock of Ecuador. International Bamboo and Rattan Network INBAR. In *Ecuador: Estrategia Nacional del Bambú*; Ministry of Agriculture and Livestock of Ecuador: Quito, Ecuador, 2018.
45. Añasco, M.; Rojas, S. *Estudio de La Cadena Desde La Producción Al Consumo del Bambú en Ecuador Con Énfasis en La Especie Guadua Angustifolia*; Ministry of Agriculture and Livestock of Ecuador: Quito, Ecuador, 2015.
46. Gatóo, A.; Sharma, B.; Bock, M.; Mulligan, H.; Ramage, M.H. Sustainable Structures: Bamboo Standards and Building Codes. *Proc. Inst. Civ. Eng. Eng. Sustain.* **2014**, *167*, 189–196. [[CrossRef](#)]
47. Dehkoda, A.M.; Ellis, N. Biochar-Based Catalyst for Simultaneous Reactions of Esterification and Transesterification. *Catal. Today* **2013**, *207*, 86–92. [[CrossRef](#)]
48. Li, M.; Zheng, Y.; Chen, Y.; Zhu, X. Biodiesel Production from Waste Cooking Oil Using a Heterogeneous Catalyst from Pyrolyzed Rice Husk. *Bioresour. Technol.* **2014**, *154*, 345–348. [[CrossRef](#)] [[PubMed](#)]
49. Houben, D.; Evrard, L.; Sonnet, P. Mobility, Bioavailability and PH-Dependent Leaching of Cadmium, Zinc and Lead in a Contaminated Soil Amended with Biochar. *Chemosphere* **2013**, *92*, 1450–1457. [[CrossRef](#)] [[PubMed](#)]
50. Guo, M.; Song, W.; Tian, J. Biochar-Facilitated Soil Remediation: Mechanisms and Efficacy Variations. *Front. Environ. Sci.* **2020**, *8*, 183. [[CrossRef](#)]
51. Lehmann, J.; Rillig, M.C.; Thies, J.; Masiello, C.A.; Hockaday, W.C.; Crowley, D. Biochar Effects on Soil Biota—A Review. *Soil Biol. Biochem.* **2011**, *43*, 1812–1836. [[CrossRef](#)]
52. González, A.S.; Plaza, M.G.; Rubiera, F.; Pevida, C. Sustainable Biomass-Based Carbon Adsorbents for Post-Combustion CO₂ Capture. *Chem. Eng. J.* **2013**, *230*, 456–465. [[CrossRef](#)]
53. Ahmad, M.; Rajapaksha, A.U.; Lim, J.E.; Zhang, M.; Bolan, N.; Mohan, D.; Vithanage, M.; Lee, S.S.; Ok, Y.S. Biochar as a Sorbent for Contaminant Management in Soil and Water: A Review. *Chemosphere* **2014**, *99*, 19–33. [[CrossRef](#)]
54. Uchimiya, M.; Wartelle, L.H.; Klasson, K.T.; Fortier, C.A.; Lima, I.M. Influence of Pyrolysis Temperature on Biochar Property and Function as a Heavy Metal Sorbent in Soil. *J. Agric. Food Chem.* **2011**, *59*, 2501–2510. [[CrossRef](#)]
55. Bardestani, R.; Patience, G.S.; Kaliaguine, S. Experimental Methods in Chemical Engineering: Specific Surface Area and Pore Size Distribution Measurements—BET, BJH, and DFT. *Can. J. Chem. Eng.* **2019**, *97*, 2781–2791. [[CrossRef](#)]
56. Villasana, Y.; Moradi, N.; Navas-Cárdenas, C.; Patience, G.S. Experimental Methods in Chemical Engineering: PH. *Can. J. Chem. Eng.* **2022**, *100*, 24393. [[CrossRef](#)]
57. Ardila, C.R.; Folgueras, M.B.; Fernández, F.J. Oxidative Pyrolysis of *Guadua Angustifolia* Kunth. *Energy Rep.* **2020**, *6*, 738–743. [[CrossRef](#)]
58. Thommes, M.; Kaneko, K.; Neimark, A.V.; Olivier, J.P.; Rodriguez-Reinoso, F.; Rouquerol, J.; Sing, K.S.W. Physisorption of Gases, with Special Reference to the Evaluation of Surface Area and Pore Size Distribution (IUPAC Technical Report). *Pure Appl. Chem.* **2015**, *87*, 1051–1069. [[CrossRef](#)]

59. Chu, G.; Zhao, J.; Huang, Y.; Zhou, D.; Liu, Y.; Wu, M.; Peng, H.; Zhao, Q.; Pan, B.; Steinberg, C.E.W. Phosphoric Acid Pretreatment Enhances the Specific Surface Areas of Biochars by Generation of Micropores. *Environ. Pollut.* **2018**, *240*, 1–9. [[CrossRef](#)] [[PubMed](#)]
60. Marsh, H.; Rodríguez-Reinoso, F. Activation Processes (Chemical). *Act. Carbon* **2006**, 322–365. [[CrossRef](#)]
61. Chen, L.; Huang, Q.; Wang, Y.; Xiao, H.; Liu, W.; Zhang, D.; Yang, T. Tailoring Performance of Co–Pt/MgO–Al₂O₃ Bimetallic Aerogel Catalyst for Methane Oxidative Carbon Dioxide Reforming: Effect of Pt/Co Ratio. *Int. J. Hydrog. Energy* **2019**, *44*, 19878–19889. [[CrossRef](#)]
62. Lastoskie, C.; Gubbins, K.E.; Quirke, N. Pore Size Distribution Analysis of Microporous Carbons: A Density Functional Theory Approach. *J. Phys. Chem.* **1993**, *97*, 4786–4796. [[CrossRef](#)]
63. Marsh, H.; Rodríguez-Reinoso, F. Porosity in Carbons: Modeling. In *Activated Carbon*; Elsevier: Amsterdam, The Netherlands, 2006; pp. 87–142. [[CrossRef](#)]
64. Qian, K.; Kumar, A.; Zhang, H.; Bellmer, D.; Huhnke, R. Recent Advances in Utilization of Biochar. *Renew. Sustain. Energy Rev.* **2015**, *42*, 1055–1064. [[CrossRef](#)]
65. Wang, Y.; Hu, Y.J.; Hao, X.; Peng, P.; Shi, J.Y.; Peng, F.; Sun, R.C. Hydrothermal Synthesis and Applications of Advanced Carbonaceous Materials from Biomass: A Review. *Adv. Compos. Hybrid Mater.* **2020**, *3*, 267–284. [[CrossRef](#)]
66. Da Medeiros, D.C.C.S.; Nzediegwu, C.; Benally, C.; Messele, S.A.; Kwak, J.H.; Naeth, M.A.; Ok, Y.S.; Chang, S.X.; Gamal El-Din, M. Pristine and Engineered Biochar for the Removal of Contaminants Co-Existing in Several Types of Industrial Wastewaters: A Critical Review. *Sci. Total Environ.* **2022**, *809*, 151120. [[CrossRef](#)]
67. Gupta, S.; Sireesha, S.; Sreedhar, I.; Patel, C.M.; Anitha, K.L. Latest Trends in Heavy Metal Removal from Wastewater by Biochar Based Sorbents. *J. Water Process Eng.* **2020**, *38*, 101561. [[CrossRef](#)]
68. Shakoor, M.B.; Ali, S.; Rizwan, M.; Abbas, F.; Bibi, I.; Riaz, M.; Khalil, U.; Niazi, N.K.; Rinklebe, J. A Review of Biochar-Based Sorbents for Separation of Heavy Metals from Water. *Int. J. Phytoremediat.* **2020**, *22*, 111–126. [[CrossRef](#)]
69. Brunelle, J.P. Preparation of Catalysts by Metallic Complex Adsorption on Mineral Oxides. *Pure Appl. Chem.* **1978**, *50*, 1211–1229. [[CrossRef](#)]
70. Kosmulski, M. Compilation of PZC and IEP of Sparingly Soluble Metal Oxides and Hydroxides from Literature. *Adv. Colloid Interface Sci.* **2009**, *152*, 14–25. [[CrossRef](#)] [[PubMed](#)]
71. Nguyen, T.H.; Pham, T.H.; Nguyen Thi, H.T.; Nguyen, T.N.; Nguyen, M.V.; Tran Dinh, T.; Nguyen, M.P.; Do, T.Q.; Phuong, T.; Hoang, T.T.; et al. Synthesis of Iron-Modified Biochar Derived from Rice Straw and Its Application to Arsenic Removal. *J. Chem.* **2019**, *2019*, 5295610. [[CrossRef](#)]
72. Chen, W.; Zhao, B.; Guo, Y.; Guo, Y.; Zheng, Z.; Pak, T.; Li, G. Effect of Hydrothermal Pretreatment on Pyrolyzed Sludge Biochars for Tetracycline Adsorption. *J. Environ. Chem. Eng.* **2021**, *9*, 106557. [[CrossRef](#)]
73. Mukherjee, A.; Zimmerman, A.R.; Harris, W. Surface Chemistry Variations among a Series of Laboratory-Produced Biochars. *Geoderma* **2011**, *163*, 247–255. [[CrossRef](#)]
74. Wu, L.; Zhao, X.; Bi, E. Predicting the Effect of Dissolved Humic Acid on Sorption of Benzotriazole to Biochar. *Biochar* **2022**, *4*, 15. [[CrossRef](#)]
75. Huang, X.; Liu, Y.; Liu, S.; Li, Z.; Tan, X.; Ding, Y.; Zeng, G.; Xu, Y.; Zeng, W.; Zheng, B. Removal of Metformin Hydrochloride by: Alternanthera Philoxeroides Biomass Derived Porous Carbon Materials Treated with Hydrogen Peroxide. *RSC Adv.* **2016**, *6*, 79275–79284. [[CrossRef](#)]
76. Gai, C.; Guo, Y.; Peng, N.; Liu, T.; Liu, Z. N-Doped Biochar Derived from Co-Hydrothermal Carbonization of Rice Husk and: Chlorella Pyrenoidosa for Enhancing Copper Ion Adsorption. *RSC Adv.* **2016**, *6*, 53713–53722. [[CrossRef](#)]
77. Saha, N.; Saba, A.; Reza, M.T. Effect of Hydrothermal Carbonization Temperature on PH, Dissociation Constants, and Acidic Functional Groups on Hydrochar from Cellulose and Wood. *J. Anal. Appl. Pyrolysis* **2019**, *137*, 138–145. [[CrossRef](#)]
78. Tran, H.N.; You, S.J.; Chao, H.P. Effect of Pyrolysis Temperatures and Times on the Adsorption of Cadmium onto Orange Peel Derived Biochar. *Waste Manag. Res.* **2016**, *34*, 129–138. [[CrossRef](#)] [[PubMed](#)]
79. Zhou, J.; Chen, H.; Thring, R.W.; Arocena, J.M. Chemical Pretreatment of Rice Straw Biochar: Effect on Biochar Properties and Hexavalent Chromium Adsorption. *Int. J. Environ. Res.* **2019**, *13*, 91–105. [[CrossRef](#)]
80. Jedynek, K.; Charnas, B. Preparation and Characterization of Physicochemical Properties of Spruce Cone Biochars Activated by CO₂. *Materials* **2021**, *14*, 3859. [[CrossRef](#)]
81. Singh, P.; Sarswat, A.; Pittman, C.U.; Mlsna, T.; Mohan, D. Sustainable Low-Concentration Arsenite [As(III)] Removal in Single and Multicomponent Systems Using Hybrid Iron Oxide-Biochar Nanocomposite Adsorbents—A Mechanistic Study. *ACS Omega* **2020**, *5*, 2575–2593. [[CrossRef](#)] [[PubMed](#)]
82. Oh, S.Y.; Seo, Y.D. Sorption of Halogenated Phenols and Pharmaceuticals to Biochar: Affecting Factors and Mechanisms. *Environ. Sci. Pollut. Res.* **2016**, *23*, 951–961. [[CrossRef](#)]
83. Trakal, L.; Veselská, V.; Šafařík, I.; Vítková, M.; Číhalová, S.; Komárek, M. Lead and Cadmium Sorption Mechanisms on Magnetically Modified Biochars. *Bioresour. Technol.* **2016**, *203*, 318–324. [[CrossRef](#)]
84. Burbano-Patiño, A.A.; Lassalle, V.L.; Horst, M.F. Magnetic Hydrochar Nanocomposite Obtained from Sunflower Husk: A Potential Material for Environmental Remediation. *J. Mol. Struct.* **2021**, *1239*, 130509. [[CrossRef](#)]
85. Zhang, H.; Hay, A.G. Magnetic Biochar Derived from Biosolids via Hydrothermal Carbonization: Enzyme Immobilization, Immobilized-Enzyme Kinetics, Environmental Toxicity. *J. Hazard. Mater.* **2020**, *384*, 121272. [[CrossRef](#)]

86. Kazak, O.; Tor, A. In Situ Preparation of Magnetic Hydrochar by Co-Hydrothermal Treatment of Waste Vinasse with Red Mud and Its Adsorption Property for Pb(II) in Aqueous Solution. *J. Hazard. Mater.* **2020**, *393*, 122391. [[CrossRef](#)]
87. Lou, Y.; Joseph, S.; Li, L.; Graber, E.R.; Liu, X.; Pan, G. Water Extract from Straw Biochar Used for Plant Growth Promotion: An Initial Test. *BioResources* **2016**, *11*, 249–266. [[CrossRef](#)]
88. Leithaeuser, A.; Gerber, M.; Span, R.; Schwede, S. Bioresource Technology Comparison of Pyrochar, Hydrochar and Lignite as Additive in Anaerobic Digestion and NH₄⁺ Adsorbent. *Bioresour. Technol.* **2022**, *361*, 127674. [[CrossRef](#)] [[PubMed](#)]
89. Wang, Y.; Wang, L.; Deng, X.; Gao, H. A Facile Pyrolysis Synthesis of Biochar/ZnO Passivator: Immobilization Behavior and Mechanisms for Cu (II) in Soil. *Environ. Sci. Pollut. Res.* **2020**, *27*, 1888–1897. [[CrossRef](#)] [[PubMed](#)]
90. Gargiulo, V.; Gomis-Berenguer, A.; Giudicianni, P.; Ania, C.O.; Ragucci, R.; Alfè, M. Assessing the Potential of Biochars Prepared by Steam-Assisted Slow Pyrolysis for CO₂ Adsorption and Separation. *Energy Fuels* **2018**, *32*, 10218–10227. [[CrossRef](#)] [[PubMed](#)]
91. Kwan, Y.C.G.; Ng, G.M.; Huan, C.H.A. Identification of Functional Groups and Determination of Carboxyl Formation Temperature in Graphene Oxide Using the XPS O 1s Spectrum. *Thin Solid Film.* **2015**, *590*, 40–48. [[CrossRef](#)]
92. Yang, X.; Liu, Z.; Jiang, Y.; Li, F.; Xue, B.; Dong, Z.; Ding, M.; Chen, R.; Yang, Q.; An, T.; et al. Micro-Structure, Surface Properties and Adsorption Capacity of Ball-Milled Cellulosic Biomass Derived Biochar Based Mineral Composites Synthesized via Carbon-Bed Pyrolysis. *Appl. Clay Sci.* **2020**, *199*, 105877. [[CrossRef](#)]
93. Zhang, S.; Yang, X.; Liu, L.; Ju, M.; Zheng, K. Adsorption Behavior of Selective Recognition Functionalized Biochar to Cd(II) in Wastewater. *Materials* **2018**, *11*, 299. [[CrossRef](#)]
94. Huson, M.G.; Church, J.S.; Kafi, A.A.; Woodhead, A.L.; Khoo, J.; Kiran, M.S.R.N.; Bradby, J.E.; Fox, B.L. Heterogeneity of Carbon Fibre. *Carbon N. Y.* **2014**, *68*, 240–249. [[CrossRef](#)]
95. Zhang, P.; Wang, X.; Xue, B.; Huang, P.; Hao, Y.; Tang, J.; Maletić, S.P.; Rončević, S.D.; Sun, H. Preparation of Graphite-like Biochars Derived from Straw and Newspaper Based on Ball-Milling and TEMPO-Mediated Oxidation and Their Supersorption Performances to Imidacloprid and Sulfadiazine. *Chem. Eng. J.* **2021**, *411*, 128502. [[CrossRef](#)]
96. Shang, Y.; Chen, C.; Zhang, P.; Yue, Q.; Li, Y.; Gao, B.; Xu, X. Removal of Sulfamethoxazole from Water via Activation of Persulfate by Fe₃C@NCNTs Including Mechanism of Radical and Nonradical Process. *Chem. Eng. J.* **2019**, *375*, 122004. [[CrossRef](#)]
97. Gao, L.; Li, Z.; Yi, W.; Li, Y.; Zhang, P.; Zhang, A.; Wang, L. Impacts of Pyrolysis Temperature on Lead Adsorption by Cotton Stalk-Derived Biochar and Related Mechanisms. *J. Environ. Chem. Eng.* **2021**, *9*, 105602. [[CrossRef](#)]
98. Yu, J.; Feng, H.; Tang, L.; Pang, Y.; Wang, J.; Zou, J.; Xie, Q.; Liu, Y.; Feng, C.; Wang, J. Insight into the Key Factors in Fast Adsorption of Organic Pollutants by Hierarchical Porous Biochar. *J. Hazard. Mater.* **2021**, *403*, 123610. [[CrossRef](#)] [[PubMed](#)]
99. Deveci, H.; Kar, Y. Adsorption of Hexavalent Chromium from Aqueous Solutions by Bio-Chars Obtained during Biomass Pyrolysis. *J. Ind. Eng. Chem.* **2013**, *19*, 190–196. [[CrossRef](#)]
100. Chen, T.; Zhou, Z.; Han, R.; Meng, R.; Wang, H.; Lu, W. Adsorption of Cadmium by Biochar Derived from Municipal Sewage Sludge: Impact Factors and Adsorption Mechanism. *Chemosphere* **2015**, *134*, 286–293. [[CrossRef](#)] [[PubMed](#)]
101. Zhu, Y.; Liang, H.; Yu, R.; Hu, G.; Chen, F. Removal of Aquatic Cadmium Ions Using Thiourea Modified Poplar Biochar. *Water* **2020**, *12*, 1117. [[CrossRef](#)]
102. Imran, M.; Suddique, M.; Shah, G.M.; Ahmad, I.; Murtaza, B.; Shah, N.S.; Mubeen, M.; Ahmad, S.; Zakir, A.; Schotting, R.J. Kinetic and Equilibrium Studies for Cadmium Biosorption from Contaminated Water Using Cassia Fistula Biomass. *Int. J. Environ. Sci. Technol.* **2019**, *16*, 3099–3108. [[CrossRef](#)]
103. Ahmad, M.; Moon, D.H.; Vithanage, M.; Koutsospyros, A.; Lee, S.S.; Yang, J.E.; Lee, S.E.; Jeon, C.; Ok, Y.S. Production and Use of Biochar from Buffalo-Weed (*Ambrosia trifida* L.) for Trichloroethylene Removal from Water. *J. Chem. Technol. Biotechnol.* **2014**, *89*, 150–157. [[CrossRef](#)]
104. Li, B.; Yang, L.; Wang, C.; Zhang, Q.; Liu, Q.; Li, Y.; Xiao, R. Adsorption of Cd(II) from Aqueous Solutions by Rape Straw Biochar Derived from Different Modification Processes. *Chemosphere* **2017**, *175*, 332–340. [[CrossRef](#)]
105. Wang, J.; Guo, X. Adsorption Kinetic Models: Physical Meanings, Applications, and Solving Methods. *J. Hazard. Mater.* **2020**, *390*, 122156. [[CrossRef](#)]
106. Wang, S.; Kwak, J.-H.; Islam, M.S.; Naeth, M.A.; Gamal El-Din, M.; Chang, S.X. Biochar Surface Complexation and Ni(II), Cu(II), and Cd(II) Adsorption in Aqueous Solutions Depend on Feedstock Type. *Sci. Total Environ.* **2020**, *712*, 136538. [[CrossRef](#)]
107. Ho, Y.S.; McKay, G. A Comparison of Chemisorption Kinetic Models Applied to Pollutant Removal on Various Sorbents. *Process Saf. Environ. Prot.* **1998**, *76*, 332–340. [[CrossRef](#)]
108. Idrees, M.; Batool, S.; Kalsoom, T.; Yasmeen, S.; Kalsoom, A.; Raina, S.; Zhuang, Q.; Kong, J. Animal Manure-Derived Biochars Produced via Fast Pyrolysis for the Removal of Divalent Copper from Aqueous Media. *J. Environ. Manage.* **2018**, *213*, 109–118. [[CrossRef](#)] [[PubMed](#)]
109. Wu, F.-C.; Tseng, R.-L.; Juang, R.-S. Characteristics of Elovich Equation Used for the Analysis of Adsorption Kinetics in Dye-Chitosan Systems. *Chem. Eng. J.* **2009**, *150*, 366–373. [[CrossRef](#)]
110. Moussout, H.; Ahlafi, H.; Aazza, M.; Maghat, H. Critical of Linear and Nonlinear Equations of Pseudo-First Order and Pseudo-Second Order Kinetic Models. *Karbala Int. J. Mod. Sci.* **2018**, *4*, 244–254. [[CrossRef](#)]
111. Romero-Cano, L.A.; García-Rosero, H.; Gonzalez-Gutierrez, L.V.; Baldenegro-Pérez, L.A.; Carrasco-Marín, F. Functionalized Adsorbents Prepared from Fruit Peels: Equilibrium, Kinetic and Thermodynamic Studies for Copper Adsorption in Aqueous Solution. *J. Clean. Prod.* **2017**, *162*, 195–204. [[CrossRef](#)]

112. Saeed, A.A.H.; Harun, N.Y.; Sufian, S.; Bilad, M.R.; Zakaria, Z.Y.; Jagaba, A.H.; Abdulhakim, A.; Ghaleb, S.; Mohammed, H.G. Pristine and Magnetic Kenaf Fiber Biochar for Cd²⁺ Adsorption from Aqueous Solution. *Int. J. Environ. Res. Public Health* **2021**, *18*, 7949. [[CrossRef](#)]
113. Naiya, T.K.; Bhattacharya, A.K.; Das, S.K. Removal of Cd(II) from Aqueous Solutions Using Clarified Sludge. *J. Colloid Interface Sci.* **2008**, *325*, 48–56. [[CrossRef](#)]
114. Langmuir, I. The Adsorption of Gases on Plane Surfaces of Glass, Mica and Platinum. *J. Am. Chem. Soc.* **1918**, *40*, 1361–1403. [[CrossRef](#)]
115. Freundlich, H.M.F. Over the Adsorption in Solution. *J. Phys. Chem* **1906**, *57*, 1100–1107.
116. Temkin, M.I. Adsorption Equilibrium and the Kinetics of Processes on Nonhomogeneous Surfaces and in the Interaction between Adsorbed Molecules. *Zh. Fiz. Chim.* **1941**, *15*, 296–332.
117. Kumar, P.; Kumar, P. Removal of Cadmium (Cd-II) from Aqueous Solution Using Gas Industry-Based Adsorbent. *SN Appl. Sci.* **2019**, *1*, 872. [[CrossRef](#)]
118. Abedpour, M.; Kamyab Moghadas, B.; Tamjidi, S. Equilibrium and Kinetic Study of Simultaneous Removal of Cd(II) and Ni(II) by Acrylamide-Based Polymer as Effective Adsorbent: Optimisation by Response Surface Methodology (RSM). *Int. J. Environ. Anal. Chem.* **2022**, *102*, 3524–3541. [[CrossRef](#)]
119. Yousif, A.M.; El-Afandy, A.H.; Abdel Wahab, G.M.; Mubark, A.E.; Ibrahim, I.A. Selective Separation of Uranium(VI) from Aqueous Solutions Using Amine Functionalized Cellulose. *J. Radioanal. Nucl. Chem.* **2015**, *303*, 1821–1833. [[CrossRef](#)]
120. Mohan, D.; Pittman, C.U.; Bricka, M.; Smith, F.; Yancey, B.; Mohammad, J.; Steele, P.H.; Alexandre-Franco, M.F.; Gómez-Serrano, V.; Gong, H. Sorption of Arsenic, Cadmium, and Lead by Chars Produced from Fast Pyrolysis of Wood and Bark during Bio-Oil Production. *J. Colloid Interface Sci.* **2007**, *310*, 57–73. [[CrossRef](#)] [[PubMed](#)]
121. Morales-Simfors, N.; Bundschuh, J.; Herath, I.; Inguaggiato, C.; Caselli, A.T.; Tapia, J.; Choquehuayta, F.E.A.; Armienta, M.A.; Ormachea, M.; Joseph, E.; et al. Arsenic in Latin America: A Critical Overview on the Geochemistry of Arsenic Originating from Geothermal Features and Volcanic Emissions for Solving Its Environmental Consequences. *Sci. Total Environ.* **2020**, *716*, 135564. [[CrossRef](#)] [[PubMed](#)]
122. Inguaggiato, S.; Hidalgo, S.; Beate, B.; Bourquin, J. Geochemical and Isotopic Characterization of Volcanic and Geothermal Fluids Discharged from the Ecuadorian Volcanic Arc. *Geofluids* **2010**, *10*, 525–541. [[CrossRef](#)]
123. Inyang, M.I.; Gao, B.; Yao, Y.; Xue, Y.; Zimmerman, A.; Mosa, A.; Pullammanappallil, P.; Ok, Y.S.; Cao, X. A Review of Biochar as a Low-Cost Adsorbent for Aqueous Heavy Metal Removal. *Crit. Rev. Environ. Sci. Technol.* **2016**, *46*, 406–433. [[CrossRef](#)]
124. Deng, Y.; Li, X.; Ni, F.; Liu, Q.; Yang, Y.; Wang, M.; Ao, T.; Chen, W. Synthesis of Magnesium Modified Biochar for Removing Copper, Lead and Cadmium in Single and Binary Systems from Aqueous Solutions: Adsorption Mechanism. *Water* **2021**, *13*, 599. [[CrossRef](#)]
125. Park, C.M.; Han, J.; Chu, K.H.; Al-Hamadani, Y.A.J.; Her, N.; Heo, J.; Yoon, Y. Influence of Solution PH, Ionic Strength, and Humic Acid on Cadmium Adsorption onto Activated Biochar: Experiment and Modeling. *J. Ind. Eng. Chem.* **2017**, *48*, 186–193. [[CrossRef](#)]
126. Banerjee, S.; Barman, S.; Halder, G. Sorptive Elucidation of Rice Husk Ash Derived Synthetic Zeolite towards Deionization of Coalmine Waste Water: A Comparative Study. *Groundw. Sustain. Dev.* **2017**, *5*, 137–151. [[CrossRef](#)]
127. Sakhiya, A.K.; Baghel, P.; Anand, A.; Vijay, V.K.; Kaushal, P. A Comparative Study of Physical and Chemical Activation of Rice Straw Derived Biochar to Enhance Zn²⁺ Adsorption. *Bioresour. Technol. Rep.* **2021**, *15*, 100774. [[CrossRef](#)]
128. Campbell, R.M.; Anderson, N.M.; Daugaard, D.E.; Naughton, H.T. Financial Viability of Biofuel and Biochar Production from Forest Biomass in the Face of Market Price Volatility and Uncertainty. *Appl. Energy* **2018**, *230*, 330–343. [[CrossRef](#)]
129. Nematian, M.; Keske, C.; Ng'ombe, J.N. A Techno-Economic Analysis of Biochar Production and the Bioeconomy for Orchard Biomass. *Waste Manag.* **2021**, *135*, 467–477. [[CrossRef](#)] [[PubMed](#)]
130. Sahoo, K.; Bilek, E.; Bergman, R.; Mani, S. Techno-Economic Analysis of Producing Solid Biofuels and Biochar from Forest Residues Using Portable Systems. *Appl. Energy* **2019**, *235*, 578–590. [[CrossRef](#)]
131. Li, F.; Cao, X.; Zhao, L.; Wang, J.; Ding, Z. Effects of Mineral Additives on Biochar Formation: Carbon Retention, Stability, and Properties. *Environ. Sci. Technol.* **2014**, *48*, 11211–11217. [[CrossRef](#)]
132. Rosas, J.M.; Ruiz-Rosas, R.; Rodríguez-Mirasol, J.; Cordero, T. Kinetic Study of the Oxidation Resistance of Phosphorus-Containing Activated Carbons. *Carbon N. Y.* **2012**, *50*, 1523–1537. [[CrossRef](#)]
133. Zhao, L.; Zheng, W.; Mašek, O.; Chen, X.; Gu, B.; Sharma, B.K.; Cao, X. Roles of Phosphoric Acid in Biochar Formation: Synchronously Improving Carbon Retention and Sorption Capacity. *J. Environ. Qual.* **2017**, *46*, 393–401. [[CrossRef](#)]
134. Niu, H.; Jin, H.; Sun, Q.; Shi, Y.; Zhang, X.; Cai, Y. Activation of Biochars by Waste Phosphoric Acids: An Integrated Disposal Route of Waste Acids and Solid Waste. *ACS Sustain. Chem. Eng.* **2021**, *9*, 16403–16414. [[CrossRef](#)]
135. Kumar, A.; Jena, H.M. Preparation and Characterization of High Surface Area Activated Carbon from Fox Nut (*Euryale ferox*) Shell by Chemical Activation with H₃PO₄. *Results Phys.* **2016**, *6*, 651–658. [[CrossRef](#)]
136. Yihunu, E.W.; Minale, M.; Abebe, S.; Limin, M. Preparation, Characterization and Cost Analysis of Activated Biochar and Hydrochar Derived from Agricultural Waste: A Comparative Study. *SN Appl. Sci.* **2019**, *1*, 873. [[CrossRef](#)]
137. Chakraborty, P.; Show, S.; Banerjee, S.; Halder, G. Mechanistic Insight into Sorptive Elimination of Ibuprofen Employing Bi-Directional Activated Biochar from Sugarcane Bagasse: Performance Evaluation and Cost Estimation. *J. Environ. Chem. Eng.* **2018**, *6*, 5287–5300. [[CrossRef](#)]

Disclaimer/Publisher's Note: The statements, opinions and data contained in all publications are solely those of the individual author(s) and contributor(s) and not of MDPI and/or the editor(s). MDPI and/or the editor(s) disclaim responsibility for any injury to people or property resulting from any ideas, methods, instructions or products referred to in the content.